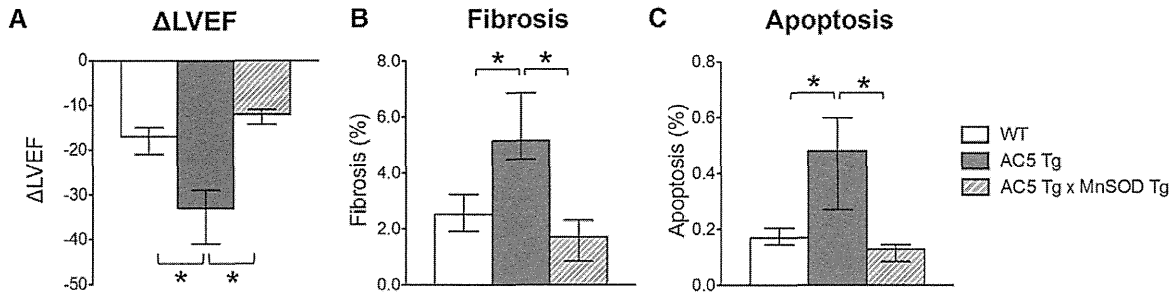

Figure 1. Chronic ISO cardiomyopathy in AC5 Tg, compared with WT, was rescued by mating the AC5 Tg mice with MnSOD Tg (AC5 Tg×MnSOD Tg) mice. *P<0.05. **A**, Delta LV ejection fraction (EF) after ISO. AC5 Tg mice fell significantly more than that of WT mice, P<0.05. In the bigenic mice the fall in LVEF was significantly less, n=6–7 per group. **B**, More fibrosis, P<0.05, was detected in AC5 Tg mice after ISO than in the other 2 groups after ISO, n=5 per group. **C**, Myocyte apoptosis, calculated by the percentage of total myocyte nuclei, also increased more in AC5 Tg than the other 2 groups. The data in **A–C** did not have a normal distribution. and the appropriate statistical tests were used (see statistical analysis section). *P<0.05. AC indicates adenylyl cyclase; ISO, isoproterenol; LV, left ventricular; MnSOD, manganese superoxide dismutase; Tg, transgenic; and WT, wild type.

AC5 Downregulates MnSOD

By Western blotting, the protein expression of MnSOD was reduced 38% in AC5 Tg mice compared with WT (Figure 3A). On the cellular level, 26% less MnSOD was detected in AC5 OE myocytes and MnSOD protein was increased 2-fold and mRNA 3.6-fold in AC5 KD myocytes (Figure 3B, 3C, and 3D). The data demonstrated that AC5 regulated the protein and mRNA expression level of MnSOD, which altered MnSOD function.

MnSOD Overexpression Ameliorated Chronic ISO Cardiomyopathy in AC5 Tg

We increased MnSOD in AC5 Tg using a bigenic (AC5 Tg×MnSOD Tg) mouse. The cardiac-specific MnSOD Tg mice had a 20-fold increase in SOD activity in the heart.[21] Baseline LVEF was similar in AC5 Tg×MnSOD Tg mice (85 [84–89] %) and AC5 Tg mice (78 [75–81] %). After chronic ISO, the LVEF of bigenic mice decreased significantly less (Figure 1A, Table I in the online-only Data Supplement),

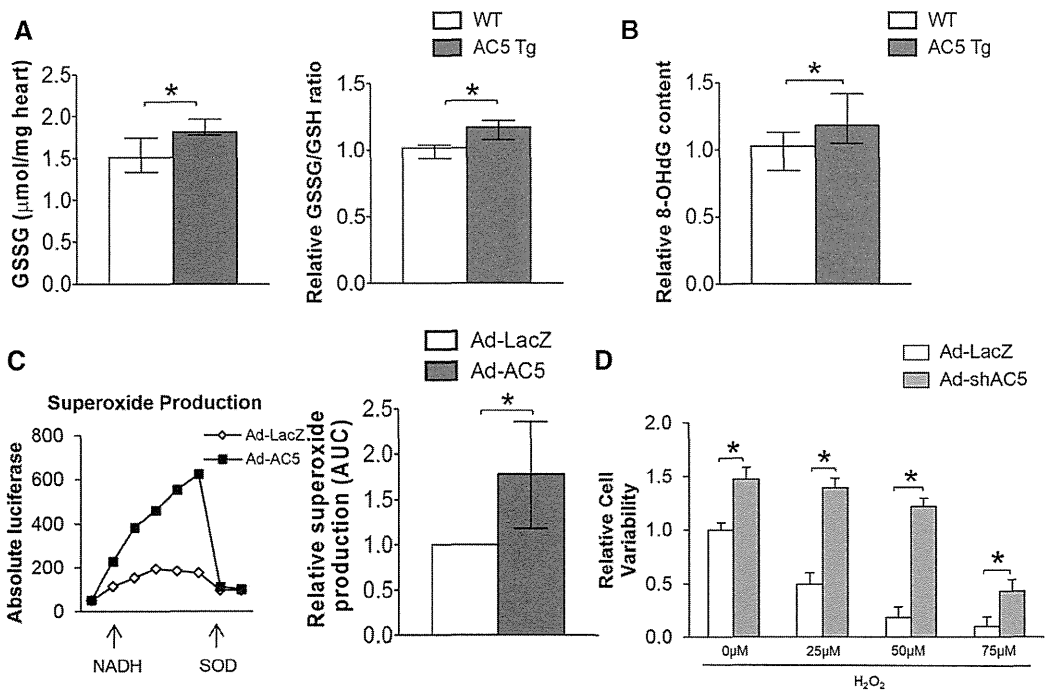

Figure 2. Oxidative stress was detected in AC5 Tg mice. **A**, Higher GSSG content (**left**), as well as GSSG/GSH ratio (**right**), were detected in AC5 Tg heart after chronic ISO stimulation. n=5 per group. **B**, The elevation of oxidative stress in AC5 Tg heart after chronic ISO stimulation was further confirmed by 8-hydroxy-2′-deoxyguanosine (8-OHdG; a marker of oxidative DNA damage) ELISA assay. n=7 per group. **C**, Ad-AC5–infected myocytes released ≈2-fold more superoxide radicals than control myocytes. n=4. **D**, Knocking down AC5 improved cell survival in myocytes treated with various concentrations of H_2O_2. n=8. The data in **A**, **B**, and **C** did not have a normal distribution, and the appropriate statistical tests were used (see Statistical Analysis section). The data in **D** had a normal distribution and were presented as mean±SEM. *P<0.05 by 1-way ANOVA with Student-Newman-Keuls post hoc analysis. *P<0.05. AC indicates adenylyl cyclase; GSH, glutathione; GSSG, glutathione disulfide; ISO indicates isoproterenol; and Tg, transgenic.

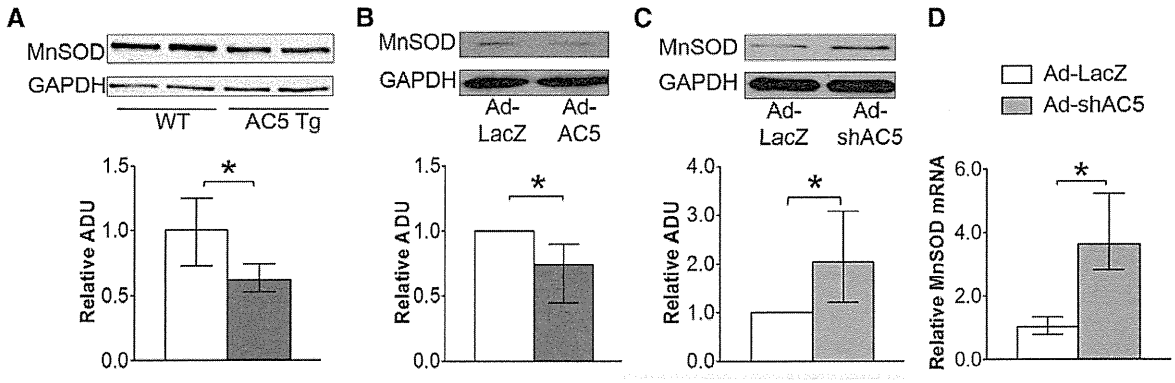

Figure 3. AC5 regulated MnSOD expression in protein and mRNA levels. **A** and **B**, Downregulation of MnSOD in AC5 Tg mice hearts (n=6 per group) and Ad-AC5–infected myocytes (n=4). **C**, MnSOD was upregulated in Ad-shAC5–infected myocytes, n=4. **D**, mRNA also increased in AC5 knockdown myocytes, n=9 per group. The data in **A–D** did not have a normal distribution, and the appropriate statistical tests were used (see Statistical Analysis section). *P<0.05. AC indicates adenylyl cyclase; MnSOD, manganese superoxide dismutase; and Tg, transgenic.

P=0.0033, to 74(66–77)%, than in AC5 Tg (45[30–49] %) mice (Figure 1A, Table I in the online-only Data Supplement). The increases in LVEDD and LVESD were also no longer greater than observed in WT (Table I in the online-only Data Supplement), and the increases in fibrosis and apoptosis, observed in AC5 Tg on chronic ISO, were no longer observed in

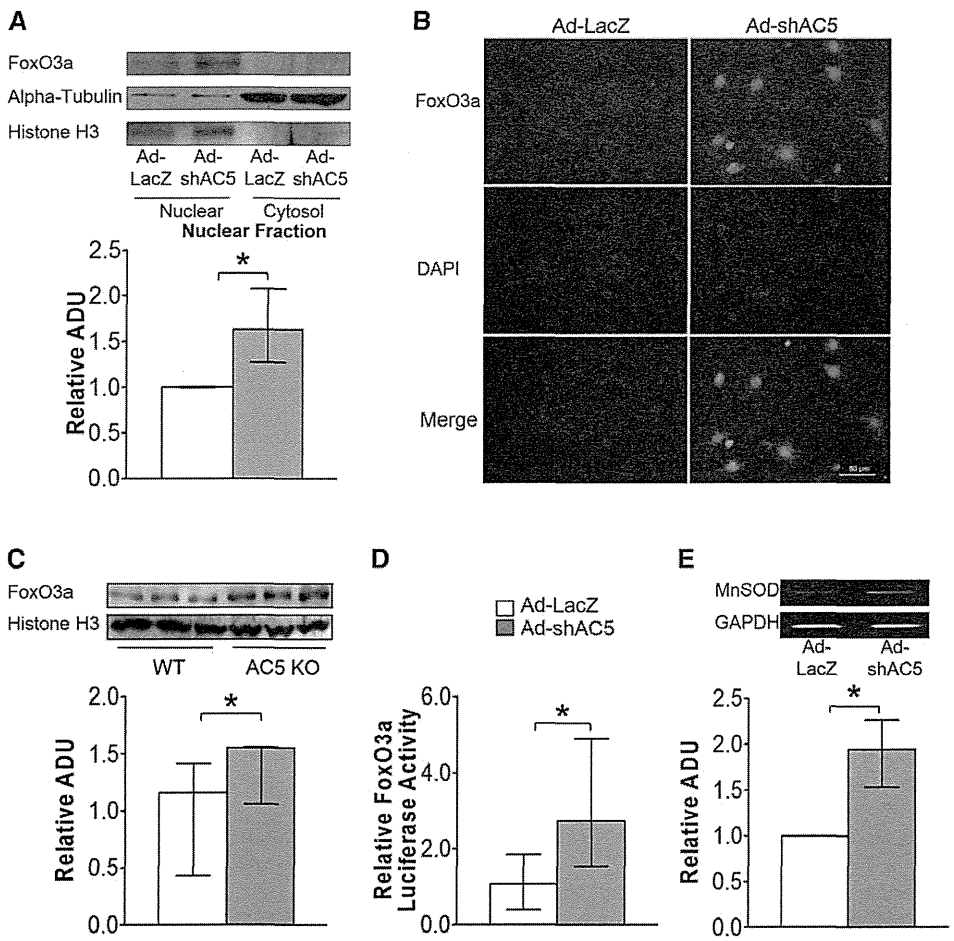

Figure 4. AC5 regulated MnSOD transcriptionally through FoxO3a. **A** and **B**, Both immunostaining (40×) and Western blotting confirm the nuclear localization of FoxO3a in AC5 KD myocytes, n=4. The data are normalized to the intensity of histone H3. **C**, More FoxO3a expression was detected in the nuclear fraction of AC5 KO heart, n=3 per group. **D**, Myocytes infected with Ad-shAC5 showed significantly higher transcriptional activity compared with Ad-LacZ infected cells, n=9 per group. **E**, Twofold more FoxO3a binding to the MnSOD promoter in AC5 KD cells compared with LacZ control cells, n=3. The data in **A–E** did not have a normal distribution, and the appropriate statistical tests were used (see Statistical Analysis section), *P<0.05. AC indicates adenylyl cyclase; KD, knockdown; KO, knockout; and MnSOD, manganese superoxide dismutase.

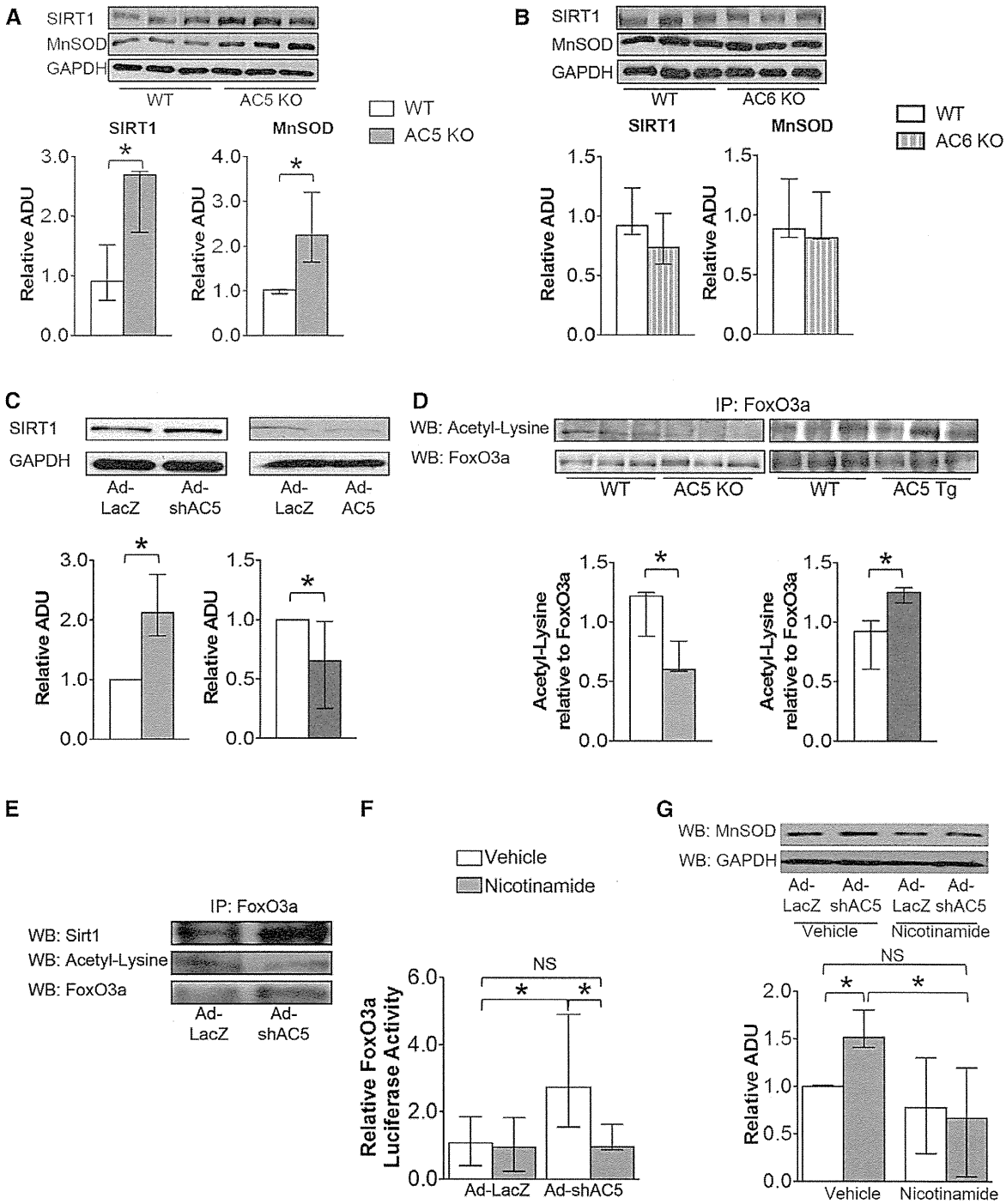

Figure 5. AC5 regulated FoxO3a transcriptional activity through SIRT1. **A**, SIRT1 and MnSOD expression levels increased in AC5 KO heart, n=3 per group, but not in AC6 KO hearts, n=3 per group (**B**). **C**, SIRT1 expression levels increased in AC5 KD cardiomyocytes (**left**; n=4) and decreased in AC5 OE cardiomyocytes (**right**; n=5). **D**, Acetyl-lysine in FoxO3a was downregulated in AC5 KO mice heart (**left**), but upregulated in AC5 Tg mouse heart (**right**), n=3 per group. **E**, Coimmunoprecipitation confirmed that SIRT1 deacetylated FoxO3a by directly binding to FoxO3a in AC5 KD cardiomyocytes. **F**, FoxO3a transcriptional activity was inhibited in AC5 KD myocytes treated with nicotinamide, a Sirtuin inhibitor, n=9 per group. The FoxO3a transcriptional activity of AC5 KD myocytes treated with nicotinamide showed no significant difference compared with cardiomyocytes infected with ad-LacZ, NS=nonsignificant. **G**, MnSOD expression level was inhibited in AC5 KD cardiomyocytes when the cells were treated with nicotinamide. n=6. The data in **A**–**G** did not have a normal distribution. The appropriate statistical tests are noted in the Statistical Analysis section. *P<0.05. AC indicates adenylyl cyclase; KD, knockdown; KO, knockout; and MnSOD, manganese superoxide dismutase.

the bigenic mice (Figure 1B and 1C). Similarly, Tempol, which also protects against oxidative stress, rescued the adverse effects of the AC5 Tg after chronic ISO stimulation (ie, the LVEF in AC5 Tg with ISO and Tempol [63(43–69)%] was higher than with ISO in AC5 Tg without Tempol [45(30–49)%]). Thus, these data demonstrated that downregulation of MnSOD in AC5 Tg mice is a key mechanism mediating the exacerbated cardiomyopathy induced by chronic ISO.

Downregulation of MnSOD Eliminated Protective Effects of AC5 KO Under Chronic Catecholamine Stress

To investigate whether MnSOD was important for the protective effects of AC5 KO mice, we crossed the AC5 KO mice with MnSOD heterozygous KO mice. Previously, we reported that the AC5 KO mice were protected against catecholamine stress.[10] This was confirmed in the present study in a small cohort, where the fall in LVEF was less in the AC5 KO than WT with chronic ISO. This protection was lost in the bigenic mice, where LVEF after chronic ISO was decreased to 50 (43–60)% (n=6), which was almost identical to the LVEF in the WT mice (53 [39–62] %, n=11; Table I in the online-only Data Supplement). Fibrosis, an indicator of the cardiomyopathy with chronic ISO, was increased similarly in WT (2.69 [1.64–3.84] %) and AC5 KO×MnSOD$^{+/-}$ mice (2.92 [2.32–3.85] %) compared with AC5 KO mice with chronic ISO (1.13 [0.81–1.37] %).

AC5 Regulated MnSOD Transcriptionally Through the SIRT1/FoxO3a Pathway

Because downregulation of MnSOD is the key mechanism mediating the enhanced cardiomyopathy of AC5 Tg mice, we investigated the molecular pathway responsible. The mRNA level of MnSOD in AC5 KD myocytes was 3.6-fold higher than those infected by a control adenovirus, Ad-LacZ (Figure 3D), which suggested that transcriptional factors may be involved in the regulation of MnSOD, with FoxO3a a likely target, as noted earlier. To determine whether FoxO3a directly regulated MnSOD, we first examined the localization of FoxO3a in the AC5 KD neonatal myocytes. Immunostaining and Western blotting detected more FoxO3a in the nucleus of AC5 KD myocytes compared with the control group (Figure 4A and 4B). Similarly in tissue, more FoxO3a was detected in the nucleus of AC5 KO mouse heart compared with WT (Figure 4C).

Next, we tested the transcriptional activity of FoxO3a using a luciferase assay by transfecting a FoxO3a luciferase vector, with a promoter containing 3 repeats of the forkhead response element (FRE), into neonatal myocytes.[22] When AC5 was knocked down in myocytes, a 2.5-fold increase in luciferase activity was observed (Figure 4D). To examine whether FoxO3a increased the native MnSOD gene directly, we performed the ChIP assay on native MnSOD in the H9C2 rat cardiac myoblast cell line infected with Ad-LacZ and Ad-shAC5, respectively. We found 1.9-fold more FoxO3a binding to the specific FoxO-binding element within the MnSOD promoter region (Figure 4E) in AC5 KD myocytes. The data demonstrated that knockdown of AC5 causes FoxO3a to localize to the nucleus and associate with the MnSOD promoter.

FoxO is known to be regulated by acetylation, a modification removed by the NAD^+-responsive, metabolic sensor SIRT1.[23] To test whether AC5 regulated SIRT1 directly, protein expression of SIRT1 was detected in AC5 KO mice hearts. SIRT1 was significantly upregulated in AC5 KO mice hearts (Figure 5A). Consistent with the adult heart data, SIRT1 was upregulated in AC5 KD myocytes and downregulated in AC5 OE neonatal myocytes (Figure 5C).

To test whether this pathway was unique to AC5, we also examined AC6 KO, the other major cardiac AC isoform. In AC6 KO, SIRT1 was not upregulated (Figure 5B). Paralleling SIRT1 expression, MnSOD was not upregulated in the AC6 KO hearts. Thus, the upregulation of SIRT1 and MnSOD expression was not attributable to a general response to AC activity.

Given the apparent link between SIRT1 and FoxO3a, we found that the level of acetyl-FoxO3a in the heart of AC5 KO and AC5 Tg mice correlated inversely with the expression of SIRT1 (Figure 5D). In AC5 KD myocytes, SIRT1 was shown by coimmunoprecipitation (IP) to bind directly to FoxO3a (Figure 5E). These data suggest that FoxO3a is regulated by deacetylation in cardiac tissue and this is controlled by AC5 activity. To further investigate the role of SIRT1, we treated AC5 KD and the control group with nicotinamide, a sirtuin inhibitor, and then tested the transcriptional activity of FoxO3a in the control group. Nicotinamide did not change the activity in the control group, but reduced the transcriptional activity of FoxO3a to almost the same level in AC5 KD group as in the control group (Figure 5F). To investigate whether the elevation of luciferase activity of FoxO3a contributed to MnSOD expression, we determined MnSOD protein levels in AC5 KD myocytes. The MnSOD level in nicotinamide-treated AC5 KD myocytes was downregulated to a similar level as the control group (Figure 5G). These data indicate that the increased transcriptional activity of FoxO3a and MnSOD expression in AC5 KD myocytes is attributable to increased SIRT1 activity. In summary, AC5 inhibited SIRT1 activity, which consequently decreased the interaction between SIRT1 and FoxO3a, thus decreasing MnSOD expression, resulting in less tolerance toward stress (Figure 6).

MnSOD Also Regulated by MEK/ERK Signaling

We previously reported that both mitogen-activated protein kinase kinase/extracellular signal-regulated kinases/MnSOD (MEK/ERK/MnSOD) and Akt pathways were involved in the protective mechanism of AC5 KO.[1,10] The elevation of MnSOD in myocytes infected with AC5 KD adenovirus was eliminated by both the MEK inhibitor (PD98059; Figure IIIB in the online-only Data Supplement) and sirtuin inhibitor (nicotinamide; Figure 5G), suggesting both the MEK/ERK and SIRT1/FoxO3a pathway are involved in MnSOD regulation. Furthermore, we examined the activity of Akt (represented as p-Akt/Akt) in AC5 Tg mice after chronic ISO. In contrast to AC5 KO mice, the activity of Akt was lower in AC5 Tg than in WT mice (Figure IV in the online-only Data Supplement), indicating that the AC5 Tg failed to activate this protective mechanism induced by chronic ISO stress. Different from MnSOD basal regulation by AC5 (Figure IIIA), Akt is involved in mediating the cardiac effects after chronic ISO stimulation.

To demonstrate that MnSOD is the only antioxidant gene targeted by the AC5 regulated SIRT1/FoxO3a pathway, we examined the expression of catalase, another downstream target of FoxO3a,[24,25] and found no differences in the hearts among WT, AC5 KO, and AC5 Tg mice (Figure V in the online-only Data Supplement).

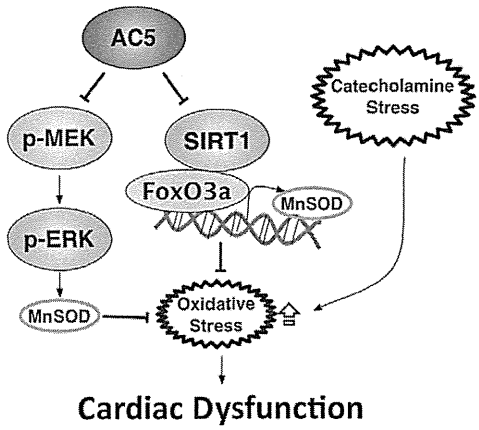

Figure 6. Signaling diagram for AC5 regulation of MnSOD through the SIRT1/FoxO3a and the MEK/ERK pathway. Imbalance between reactive oxygen species production and the intracellular antioxidant system results in the intolerance of AC5 Tg to stress. AC indicates adenylyl cyclase; MEK, mitogen-activated protein kinase kinase; ERK, extracellular signal-regulated kinases; MnSOD, manganese superoxide dismutase; and Tg, transgenic.

Discussion

Because the conclusions from previous studies examining the extent to which cardiac overexpression or deletion of AC5 affects the development of cardiomyopathy have been controversial[6,7,17,26] and no previous study examined the effects of cardiac overexpression of AC5 on the development of cardiomyopathy, the goal of the present investigation was to do just that, using the model of chronic catecholamine stress. The results indicate clearly that cardiac overexpression of AC5 increases the severity of the cardiomyopathy induced by chronic catecholamine stress, resulting in more severely compromised LV function and increased LV dilation, cardiac fibrosis, and apoptosis. It is well recognized that catecholamines increase oxidative stress, which in turn induces necrosis and results in cardiac fibrosis,[27–30] which is an important mechanism mediating the decrease in function observed, not only in the cardiomyopathy induced by chronic ISO but also in all cardiomyopathies. Although the most common cause of necrosis is myocardial ischemia, it can also result from an imbalance between myocardial oxygen supply and demand, particularly in the subendocardium, and there is also nonischemic necrosis,[27] all of which leads to a reduction in contractile units in the heart and increased fibrosis, which interferes with cardiac contraction. ISO also induces necrosis in myocytes in culture, independent of myocardial blood supply.[27,31,32]

There is another reason for controversial results in literature (ie, it is not always possible to extrapolate linearly between in vivo and in vitro work and between Tg and KO models). A major strength of this investigation was the use of both Tg and KO models for AC5, which alleviated the criticisms that the high level of overexpression of AC5 in the Tg model, overwhelmed other mechanisms. In addition, finding reciprocal data in the KO and Tg model strengthens the conclusions.

Because MnSOD protects against oxidative stress in AC5 KO mice[1] and because oxidative stress has been implicated in catecholamine induced cardiomyopathy,[11,27,33] our hypothesis was that the adverse effects of AC5 overexpression in the heart are mediated by enhanced oxidative stress, primarily through an MnSOD mechanism. Confirming this hypothesis we found a 36% decrease of MnSOD expression in AC5 Tg mice and greater oxidative stress induced DNA damage. To further confirm our hypothesis that the reduced MnSOD was responsible for the enhanced oxidative stress, we restored MnSOD to the AC5 Tg mice by mating them with MnSOD Tg mice. The bigenic mice no longer responded to chronic ISO with more severe cardiomyopathy. To further confirm our hypothesis, we also examined whether reducing MnSOD eliminated the protection afforded to AC5 KO mice. Accordingly, we also mated $MnSOD^{+/-}$ mice with AC5 KO mice and then subjected the bigenic mice to chronic ISO stimulation. The bigenic mice were no longer protected from chronic catecholamine stress. Thus, the level of expression of MnSOD was responsible for the difference in responses to chronic catecholamine stimulation from WT in AC5 Tg and AC5 KO mice, and the opposite responses in AC5 Tg and AC5 KO mice. It was important to use the KO model in parallel with the AC5 Tg model, to avoid complicating influences derived from increasing gene expression to a high level. More importantly, the elimination of the protective effect in AC5 KO×$MnSOD^{+/-}$ mice is direct evidence that indicates the importance of MnSOD in the AC5 regulatory pathway. Other studies have found that oxidative stress is an important mechanism mediating several different cardiomyopathies,[28–30,33,34] and Dai et al[35] showed the importance of mitochondrial oxidative stress. However, the signaling pathways have not been elucidated.

In this connection, it was previously shown that impaired mitochondrial function in cardiac myocytes from $Sod2^{+/-}$ mouse hearts is associated with a reduction in MnSOD activity,[36] which might suggest that the same phenomenon might occur in the AC5 Tg, where MnSOD activity is reduced, and that this may reduce cardiac function. However, we observed increased LV function at baseline in AC5 Tg and impaired function with chronic ISO. This apparent conundrum can be explained by the complex interaction of mechanisms controlling cardiac function in normal animals in vivo and more so in Tg animals. Because AC5 is a direct downstream target of the β-AR, the increased basal LV function is a result of amplifying signals from the β-AR and not attributable to reduced MnSOD expression. Chronic ISO stress in AC5 Tg leads to the accumulation of oxidative stress, and an imbalance between oxygen supply and demand in the heart, leading to necrosis, apoptosis, and fibrosis, which consequently reduced LV function and resulted in cardiomyopathy.

We then investigated the signaling pathway by which AC5 regulated MnSOD expression. In AC5 KD myocytes, we detected a significant increase in MnSOD mRNA, which suggests that AC5 also regulated MnSOD in a transcriptional manner. As noted earlier, the experiments demonstrating the role of MnSOD in mediating the enhanced cardiomyopathy with chronic ISO stress in AC5 Tg led us to investigate the SIRT1/FoxO3a pathway, in view of its protective role against oxidative stress associated with aging in *C elegans*,[13,14] rats,[15] and human quiescent cells.[16] In our study, we demonstrate for the first time the importance of AC5, an upstream gene of the SIRT1/FoxO3a complex regulating MnSOD in cardiomyopathy. We also found

activation of SIRT1 and FoxO3a in AC5 KD myocytes, whereas inhibition was detected in AC5 OE myocytes, suggesting that AC5 inhibits SIRT1 and FoxO3a activity, resulting in an impaired antioxidant system and induced cell death, suggesting that overexpression of SIRT1 or nicotinamide mononucleotide (NMN) or nicotinamide riboside treatment[37] should be able to counteract the adverse effects of increased AC5 in the setting of chronic catecholamine cardiomyopathy. These conclusions are based in part on the acetylation experiments, which have the limitation of using the immunoprecipitation technique.[38] A future direction will be to use a specific antibody for acetyl FoxO3a when it is available, which would permit a more definitive conclusion.

FoxO3a is known to regulate MnSOD transcriptionally, protecting cells from cellular oxidative stress.[16] FoxO activity is regulated, in turn, by SIRT1, which also exerts favorable effects on oxidative stress resistance in cardiac myocytes.[23] An interaction between the cAMP/PKA pathway and Sir2 (an ortholog of SIRT1) in yeast has been reported.[39] Recently, a few studies indicated cAMP/PKA dependent pathways of SIRT1 activation,[40,41] which seem to be at variance with our findings. However, there are at least 4 important differences between these studies and ours. These studies were conducted in cancer, skeletal muscle, or hepatic cells, whereas we examined cardiomyocytes. Secondly, our findings are related only to AC5; it is conceivable that other AC isoforms, even AC6, the other major isoform in the heart, could induce different regulation. Indeed, this is what we observed. Because in the studies by Noriega and Gerhart-Hines, forskolin was used to stimulate AC, which will activate all AC isoforms, this may have influenced AC6, which regulates AC activity to a greater effect than AC5 in the heart. Fourth, our study was conducted under conditions of chronic activation or inhibition of the cAMP/PKA pathway (eg, in AC5 Tg and KO) and measured the change in protein expression of SIRT1, whereas the previous studies used more acute activation of cAMP/PKA with forskolin, which activated SIRT1, either through the induction of its transcription or through SIRT1 phosphorylation. Finally, the results of our investigation relating AC5 to the SIRT1/FoxO pathway is consistent with other studies showing that SIRT1/FoxO protects the heart against oxidative stress, and that MnSOD plays an important role.[42,43] It has been shown that overexpression of SIRT1 no longer promotes cell survival when MnSOD was eliminated[42] and nuclear translocation of FoxO induced transcriptional up-regulation of MnSOD, which protected the heart from myocardial infarction.[43] In addition, we found translocation and activation of FoxO3a by SIRT1, consistent with a report in *C elegans*.[23] Because FoxO3a regulates several molecules involved in the cell cycle and oxidative stress (eg, catalase[24,25]), it is possible that MnSOD is not uniquely targeted. However, we found that catalase expression was not different in hearts from WT, AC5 Tg, and AC5 KO (Figure V in the online-only Data Supplement), supporting the concept that MnSOD is uniquely regulated by FoxO3a with relation to AC5. Deacetylation of FoxO3a should activate the transcriptional activity as described previously.[23] As shown in Figure 5F and 5G, inhibition of SIRT1 activity reduced the FoxO3a transcriptional activity and MnSOD expression in AC5 KD myocytes. Because MnSOD is one of the important downstream targets of FoxO3a, it is expected that the binding affinity to the MnSOD promoter increases as FoxO3a is activated.

It is important that we found the signaling mechanisms differed in the 2 major cardiac AC isoforms, AC5 and AC6. There have been several instances of AC isoform differences within organs. AC1, AC5, and AC8 all are major isoforms in brain, AC1 and AC8 play an important role in memory and learning,[44,45] but not AC5. Similarly, AC1 KO and AC5 KO mice are resistant to pain stress,[46,47] but not AC8. Also there are apparent differences in AC5 and AC6 regulation in the heart, showing that the AC5 KO is protected against stress,[9,10] but not AC6 KO.[48]

We previously found that the MEK/ERK pathway regulated MnSOD in the AC5 KO.[1] In the current investigation we found that MnSOD was upregulated similarly in AC5 KO mice with vehicle and with ISO (Figure IIIA in the online-only Data Supplement) and that both a MEK inhibitor and a sirtuin inhibitor blocked the elevation of MnSOD in AC5 KD myocytes (Figure 5G, Figure IIIB the online-only Data Supplement), suggesting that both of these pathways are involved in the regulation of MnSOD by AC5.

In summary, this study examined for the first time the effects of overexpression of AC5 on the response to cardiac stress. In contrast to conflicting results from previous studies in AC5 Tg,[6,7] the results of the current investigation indicate clearly that overexpression of AC5 is deleterious in response to cardiac stress. We also demonstrated a new pathway for cardiac dysfunction mediated by AC5; cardiac overexpression of AC5 exacerbates the cardiomyopathy induced by chronic catecholamine stress through a mechanism inhibiting SIRT1 and FoxO3a, which decreases MnSOD transcription. The impaired antioxidant system elevates the intercellular oxidative stress level with chronic ISO stimulation, inducing more cell death and resulting in augmented cardiac dysfunction.

Acknowledgments

We appreciate the generous gifts of the MnSOD$^{+/-}$ mouse model by Dr Ting-Ting Huang. We thank Drs Chunbo Wang and Yimin Tian for technical support of the immunohistology analyses.

Sources of Funding

This study was supported by funding from the National Institutes of Health (5R01HL093481, 1R01HL106511, 5P01AG027211, 1R01HL102472, 5R01HL033107, 5T32HL069752, 5R01HL095888, 5P01HL069020, 5R01HL091781, 5R01HL093415, 5R01AG028730, 1R01AG019719). Dr Sinclair is supported by the Glenn Foundation for Medical Research.

Disclosures

Dr Sinclair is a consultant to Sirtris, a GSK company working to develop sirtuin-targeted medicines. The other authors report no conflicts.

References

1. Yan L, Vatner DE, O'Connor JP, Ivessa A, Ge H, Chen W, Hirotani S, Ishikawa Y, Sadoshima J, Vatner SF. Type 5 adenylyl cyclase disruption increases longevity and protects against stress. *Cell*. 2007;130:247–258.

2. Hines LM, Tabakoff B; WHO/ISBRA Study on State and Trait Markers of Alcohol Use and Dependence Investigators. Platelet adenylyl cyclase activity: a biological marker for major depression and recent drug use. *Biol Psychiatry*. 2005;58:955–962.
3. El-Mowafy AM, Alkhalaf M. Resveratrol activates adenylyl-cyclase in human breast cancer cells: a novel, estrogen receptor-independent cytostatic mechanism. *Carcinogenesis*. 2003;24:869–873.
4. Hanoune J, Defer N. Regulation and role of adenylyl cyclase isoforms. *Annu Rev Pharmacol Toxicol*. 2001;41:145–174.
5. Moorman C, Plasterk RH. Functional characterization of the adenylyl cyclase gene sgs-1 by analysis of a mutational spectrum in Caenorhabditis elegans. *Genetics*. 2002;161:133–142.
6. Tepe NM, Liggett SB. Transgenic replacement of type V adenylyl cyclase identifies a critical mechanism of beta-adrenergic receptor dysfunction in the G alpha q overexpressing mouse. *FEBS Lett*. 1999;458:236–240.
7. Petrashevskaya N, Gaume BR, Mihlbachler KA, Dorn GW II, Liggett SB. Bitransgenesis with beta(2)-adrenergic receptors or adenylyl cyclase fails to improve beta(1)-adrenergic receptor cardiomyopathy. *Clin Transl Sci*. 2008;1:221–227.
8. Timofeyev V, Porter CA, Tuteja D, Qiu H, Li N, Tang T, Singapuri A, Han PL, Lopez JE, Hammond HK, Chiamvimonvat N. Disruption of adenylyl cyclase type V does not rescue the phenotype of cardiac-specific overexpression of Galphaq protein-induced cardiomyopathy. *Am J Physiol Heart Circ Physiol*. 2010;299:H1459–H1467.
9. Okumura S, Takagi G, Kawabe J, Yang G, Lee MC, Hong C, Liu J, Vatner DE, Sadoshima J, Vatner SF, Ishikawa Y. Disruption of type 5 adenylyl cyclase gene preserves cardiac function against pressure overload. *Proc Natl Acad Sci USA*. 2003;100:9986–9990.
10. Okumura S, Vatner DE, Kurotani R, Bai Y, Gao S, Yuan Z, Iwatsubo K, Ulucan C, Kawabe J, Ghosh K, Vatner SF, Ishikawa Y. Disruption of type 5 adenylyl cyclase enhances desensitization of cyclic adenosine monophosphate signal and increases Akt signal with chronic catecholamine stress. *Circulation*. 2007;116:1776–1783.
11. Zhang GX, Kimura S, Nishiyama A, Shokoji T, Rahman M, Yao L, Nagai Y, Fujisawa Y, Miyatake A, Abe Y. Cardiac oxidative stress in acute and chronic isoproterenol-infused rats. *Cardiovasc Res*. 2005;65:230–238.
12. Srivastava S, Chandrasekar B, Gu Y, Luo J, Hamid T, Hill BG, Prabhu SD. Downregulation of CuZn-superoxide dismutase contributes to beta-adrenergic receptor-mediated oxidative stress in the heart. *Cardiovasc Res*. 2007;74:445–455.
13. Lin K, Hsin H, Libina N, Kenyon C. Regulation of the Caenorhabditis elegans longevity protein DAF-16 by insulin/IGF-1 and germline signaling. *Nat Genet*. 2001;28:139–145.
14. Furuyama T, Nakazawa T, Nakano I, Mori N. Identification of the differential distribution patterns of mRNAs and consensus binding sequences for mouse DAF-16 homologues. *Biochem J*. 2000;349(Pt 2):629–634.
15. Li M, Chiu JF, Mossman BT, Fukagawa NK. Down-regulation of manganese-superoxide dismutase through phosphorylation of FOXO3a by Akt in explanted vascular smooth muscle cells from old rats. *J Biol Chem*. 2006;281:40429–40439.
16. Kops GJ, Dansen TB, Polderman PE, Saarloos I, Wirtz KW, Coffer PJ, Huang TT, Bos JL, Medema RH, Burgering BM. Forkhead transcription factor FOXO3a protects quiescent cells from oxidative stress. *Nature*. 2002;419:316–321.
17. Hu CL, Chandra R, Ge H, Pain J, Yan L, Babu G, Depre C, Iwatsubo K, Ishikawa Y, Sadoshima J, Vatner SF, Vatner DE. Adenylyl cyclase type 5 protein expression during cardiac development and stress. *Am J Physiol Heart Circ Physiol*. 2009;297:H1776–H1782.
18. Qiu H, Lizano P, Laure L, Sui X, Rashed E, Park JY, Hong C, Gao S, Holle E, Morin D, Dhar SK, Wagner T, Berdeaux A, Tian B, Vatner SF, Depre C. H11 kinase/heat shock protein 22 deletion impairs both nuclear and mitochondrial functions of STAT3 and accelerates the transition into heart failure on cardiac overload. *Circulation*. 2011;124:406–415.
19. Ago T, Kitazono T, Ooboshi H, Iyama T, Han YH, Takada J, Wakisaka M, Ibayashi S, Utsumi H, Iida M. Nox4 as the major catalytic component of an endothelial NAD(P)H oxidase. *Circulation*. 2004;109:227–233.
20. Peter PS, Brady JE, Yan L, Chen W, Engelhardt S, Wang Y, Sadoshima J, Vatner SF, Vatner DE. Inhibition of p38 alpha MAPK rescues cardiomyopathy induced by overexpressed beta 2-adrenergic receptor, but not beta 1-adrenergic receptor. *J Clin Invest*. 2007;117:1335–1343.
21. Shen X, Zheng S, Metreveli NS, Epstein PN. Protection of cardiac mitochondria by overexpression of MnSOD reduces diabetic cardiomyopathy. *Diabetes*. 2006;55:798–805.
22. Brunet A, Bonni A, Zigmond MJ, Lin MZ, Juo P, Hu LS, Anderson MJ, Arden KC, Blenis J, Greenberg ME. Akt promotes cell survival by phosphorylating and inhibiting a Forkhead transcription factor. *Cell*. 1999;96:857–868.
23. Brunet A, Sweeney LB, Sturgill JF, Chua KF, Greer PL, Lin Y, Tran H, Ross SE, Mostoslavsky R, Cohen HY, Hu LS, Cheng HL, Jedrychowski MP, Gygi SP, Sinclair DA, Alt FW, Greenberg ME. Stress-dependent regulation of FOXO transcription factors by the SIRT1 deacetylase. *Science*. 2004;303:2011–2015.
24. Nemoto S, Finkel T. Redox regulation of forkhead proteins through a p66shc-dependent signaling pathway. *Science*. 2002;295:2450–2452.
25. van der Horst A, Burgering BM. Stressing the role of FoxO proteins in lifespan and disease. *Nat Rev Mol Cell Biol*. 2007;8:440–450.
26. Iwatsubo K, Bravo C, Uechi M, Baljinnyam E, Nakamura T, Umemura M, Lai L, Gao S, Yan L, Zhao X, Park M, Qiu H, Okumura S, Iwatsubo M, Vatner DE, Vatner SF, Ishikawa Y. Prevention of heart failure in mice by an antiviral agent that inhibits type 5 cardiac adenylyl cyclase. *Am J Physiol Heart Circ Physiol*. 2012;302:H2622–H2628.
27. Khan MU, Cheema Y, Shahbaz AU, Ahokas RA, Sun Y, Gerling IC, Bhattacharya SK, Weber KT. Mitochondria play a central role in nonischemic cardiomyocyte necrosis: common to acute and chronic stressor states. *Pflugers Arch*. 2012;464:123–131.
28. Robinson AD, Ramanathan KB, McGee JE, Newman KP, Weber KT. Oxidative stress and cardiomyocyte necrosis with elevated serum troponins: pathophysiologic mechanisms. *Am J Med. Sci*. 2011;342:129–134.
29. Ungvári Z, Gupte SA, Recchia FA, Bátkai S, Pacher P. Role of oxidative-nitrosative stress and downstream pathways in various forms of cardiomyopathy and heart failure. *Curr Vasc Pharmacol*. 2005;3:221–229.
30. Wexler RK, Elton T, Pleister A, Feldman D. Cardiomyopathy: an overview. *Am Fam Physician*. 2009;79:778–784.
31. Izem-Meziane M, Djerdjouri B, Rimbaud S, Caffin F, Fortin D, Garnier A, Veksler V, Joubert F, Ventura-Clapier R. Catecholamine-induced cardiac mitochondrial dysfunction and mPTP opening: protective effect of curcumin. *Am J Physiol Heart Circ Physiol*. 2012;302:H665–H674.
32. Matzinger P. The danger model: a renewed sense of self. *Science*. 2002;296:301–305.
33. Dhalla NS, Adameova A, Kaur M. Role of catecholamine oxidation in sudden cardiac death. *Fundam Clin Pharmacol*. 2010;24:539–546.
34. Shaheen M, Cheema Y, Shahbaz AU, Bhattacharya SK, Weber KT. Intracellular calcium overloading and oxidative stress in cardiomyocyte necrosis via a mitochondriocentric signal-transducer-effector pathway. *Exp Clin Cardiol*. 2011;16:109–115.
35. Dai DF, Johnson SC, Villarin JJ, Chin MT, Nieves-Cintrón M, Chen T, Marcinek DJ, Dorn GW II, Kang YJ, Prolla TA, Santana LF, Rabinovitch PS. Mitochondrial oxidative stress mediates angiotensin II-induced cardiac hypertrophy and Galphaq overexpression-induced heart failure. *Circ Res*. 2011;108:837–846.
36. Van Remmen H, Williams MD, Guo Z, Estlack L, Yang H, Carlson EJ, Epstein CJ, Huang TT, Richardson A. Knockout mice heterozygous for Sod2 show alterations in cardiac mitochondrial function and apoptosis. *Am J Physiol Heart Circ Physiol*. 2001;281:H1422–H1432.
37. Cantó C, Houtkooper RH, Pirinen E, Youn DY, Oosterveer MH, Cen Y, Fernandez-Marcos PJ, Yamamoto H, Andreux PA, Cettour-Rose P, Gademann K, Rinsch C, Schoonjans K, Sauve AA, Auwerx J. The NAD(+) precursor nicotinamide riboside enhances oxidative metabolism and protects against high-fat diet-induced obesity. *Cell Metab*. 2012;15:838–847.
38. Qin W, Zhao W, Ho L, Wang J, Walsh K, Gandy S, Pasinetti GM. Regulation of forkhead transcription factor FoxO3a contributes to calorie restriction-induced prevention of Alzheimer's disease-type amyloid neuropathology and spatial memory deterioration. *Ann N Y Acad Sci*. 2008;1147:335–347.
39. Lin SJ, Defossez PA, Guarente L. Requirement of NAD and SIR2 for life-span extension by calorie restriction in Saccharomyces cerevisiae. *Science*. 2000;289:2126–2128.
40. Gerhart-Hines Z, Dominy JE Jr, Blättler SM, Jedrychowski MP, Banks AS, Lim JH, Chim H, Gygi SP, Puigserver P. The cAMP/PKA pathway rapidly activates SIRT1 to promote fatty acid oxidation independently of changes in NAD(+). *Mol Cell*. 2011;44:851–863.
41. Noriega LG, Feige JN, Canto C, Yamamoto H, Yu J, Herman MA, Mataki C, Kahn BB, Auwerx J. CREB and ChREBP oppositely regulate SIRT1 expression in response to energy availability. *EMBO Rep*. 2011;12:1069–1076.
42. Tanno M, Kuno A, Yano T, Miura T, Hisahara S, Ishikawa S, Shimamoto K, Horio Y. Induction of manganese superoxide dismutase by nuclear translocation and activation of SIRT1 promotes cell survival in chronic heart failure. *J Biol Chem*. 2010;285:8375–8382.

43. Sengupta A, Molkentin JD, Paik JH, DePinho RA, Yutzey KE. FoxO transcription factors promote cardiomyocyte survival upon induction of oxidative stress. *J Biol Chem*. 2011;286:7468–7478.
44. Wong ST, Athos J, Figueroa XA, Pineda VV, Schaefer ML, Chavkin CC, Muglia LJ, Storm DR. Calcium-stimulated adenylyl cyclase activity is critical for hippocampus-dependent long-term memory and late phase LTP. *Neuron*. 1999;23:787–798.
45. Wang H, Pineda VV, Chan GC, Wong ST, Muglia LJ, Storm DR. Type 8 adenylyl cyclase is targeted to excitatory synapses and required for mossy fiber long-term potentiation. *J Neurosci*. 2003;23:9710–9718.
46. Vadakkan KI, Wang H, Ko SW, Zastepa E, Petrovic MJ, Sluka KA, Zhuo M. Genetic reduction of chronic muscle pain in mice lacking calcium/calmodulin-stimulated adenylyl cyclases. *Mol Pain*. 2006;2:7.
47. Kim KS, Kim J, Back SK, Im JY, Na HS, Han PL. Markedly attenuated acute and chronic pain responses in mice lacking adenylyl cyclase-5. *Genes Brain Behav*. 2007;6:120–127.
48. Lai NC, Tang T, Gao MH, Saito M, Takahashi T, Roth DM, Hammond HK. Activation of cardiac adenylyl cyclase expression increases function of the failing ischemic heart in mice. *J Am Coll Cardiol*. 2008;51:1490–1497.

CLINICAL PERSPECTIVE

The clinical significance of this investigation goes beyond simply understanding mechanisms mediating catecholamine cardiomyopathy and the role of adenylyl cyclase, oxidative stress, and the type 5 adenylyl cyclase (AC5)/Sirt1/FoxO3a pathway. These results will have direct application to clinical conditions of elevated circulating catecholamines (eg, pheochromocytoma), but more importantly potentially for all clinical conditions of elevated sympathetic activity (eg, heart failure). Currently, β-adrenergic receptor blockers play an important role in protecting against sympathetic stress in heart failure, but their efficacy is far from perfect. AC5 is in the β-adrenergic signaling pathway but is not a β-blocker. Therefore, discovering drugs to inhibit AC5 could be a major benefit for heart failure therapy, either alone or in combination with beta blockers.

nature COMMUNICATIONS

ARTICLE

Received 23 Oct 2012 | Accepted 27 Feb 2013 | Published 9 Apr 2013

DOI: 10.1038/ncomms2673

OPEN

A role for Piezo2 in EPAC1-dependent mechanical allodynia

N. Eijkelkamp[1,2,†], J.E. Linley[1,†], J.M. Torres[1,3], L. Bee[1,4], A.H. Dickenson[4], M. Gringhuis[1], M.S. Minett[1], G.S. Hong[1,5], E. Lee[1,5], U. Oh[5], Y. Ishikawa[6], F.J. Zwartkuis[7], J.J. Cox[1] & J.N. Wood[1,5]

Aberrant mechanosensation has an important role in different pain states. Here we show that Epac1 (cyclic AMP sensor) potentiation of Piezo2-mediated mechanotransduction contributes to mechanical allodynia. Dorsal root ganglia Epac1 mRNA levels increase during neuropathic pain, and nerve damage-induced allodynia is reduced in Epac1 $-/-$ mice. The Epac-selective cAMP analogue 8-pCPT sensitizes mechanically evoked currents in sensory neurons. Human Piezo2 produces large mechanically gated currents that are enhanced by the activation of the cAMP-sensor Epac1 or cytosolic calcium but are unaffected by protein kinase C or protein kinase A and depend on the integrity of the cytoskeleton. *In vivo*, 8-pCPT induces long-lasting allodynia that is prevented by the knockdown of Epac1 and attenuated by mouse Piezo2 knockdown. Piezo2 knockdown also enhanced thresholds for light touch. Finally, 8-pCPT sensitizes responses to innocuous mechanical stimuli without changing the electrical excitability of sensory fibres. These data indicate that the Epac1–Piezo2 axis has a role in the development of mechanical allodynia during neuropathic pain.

[1] Molecular Nociception Group, Wolfson Institute for Biomedical Research, University College London, London WC1E 6BT, UK. [2] Laboratory of Neuroimmunology and Developmental Origins of Disease, University Medical Center Utrecht 3584 EA, The Netherlands. [3] Department of Biochemistry, Molecular Biology and Immunology, Faculty of Medicine, University of Granada, Granada 18012, Spain. [4] Research Department of Neuroscience, Physiology and Pharmacology, University College London, London WC1E 6BT, UK. [5] Department of Molecular Medicine and Biopharmaceutical Sciences, World Class University Program, Seoul National University, Seoul 151-742, South Korea. [6] Cardiovascular Research Institute, Yokohama City University Graduate School of Medicine, Yokohama 236-0004, Japan. [7] Department of Physiological Chemistry, University Medical Center Utrecht, Center for Biomedical Genetics and Cancer Genomics Center, Utrecht 3584 CG, The Netherlands. [†] There authors shared first authorship. Correspondence and requests for materials should be addressed to J.N.W. (email: J.Wood@ucl.ac.uk) or to N.E. (email: N.Eijkelkamp@umcutrecht.nl).

Sensory neurons innervate peripheral tissues where they transduce and transmit information about noxious and innocuous stimuli to the central nervous system[1,2]. Damage to sensory neurons as a result of chemotherapy, trauma or in diabetics and human immunodeficiency virus-infected patients may lead to neuropathic pain, often associated with mechanical allodynia, where normally innocuous stimuli such as light touch are perceived as painful[3]. The possible involvement of mechanotransducers such as Piezo or TRPC channels in the development of allodynia is a topic of interest[4,5].

Cyclic AMP is an intracellular signalling messenger that changes pain thresholds[6] through the activation of two sensors: protein kinase A (PKA) and Epac (exchange protein directly activated by cAMP)[7]. Intradermal injection of a cAMP analogue causes hypersensitivity to mechanical stimuli[6]. Importantly, mechanical allodynia in murine neuropathic pain models is severely attenuated in mice in which different adenylate cyclases, the enzyme family that generates cAMP, are genetically or pharmacologically targeted[8,9]. Interestingly, however, the downstream cAMP-sensor PKA is not required for the development of allodynia in neuropathic pain models[10,11]. The role of the cAMP-sensor Epac in the development of neuropathic pain-associated allodynia is unknown. Epac1 and Epac2 are guanine nucleotide exchange factors that activate Rap, a small GTP-binding protein of the Ras family of GTPases. The binding of cAMP or the Epac-specific agonist, 8-pCPT, stimulates Rap1 via the exchange of GDP for GTP[12,13]. Various effector proteins, including adaptor proteins that affect the cytoskeleton, regulators of G proteins of the Rho family, and phospholipases (for example, PLCε) and protein kinases, signal downstream from Rap[14].

Here we investigated the role of Epac signalling in the development of allodynia associated with neuropathic pain and the role of Piezo2 in this process. We show that the cAMP-sensor Epac1 sensitizes Piezo2 leading to allodynia. This work highlights a new pain pathway, which if successfully targeted, could potentially lead to better treatments for aspects of neuropathic pain.

Results

Epac1 expression in sensory neurons during neuropathic pain. We measured Epac1 and Epac2 mRNA expression in a neuropathic pain model. Four weeks after a unilateral L5 nerve transection (L5 SNT), mice displayed mechanical allodynia in the ipsilateral paw. Thresholds to mechanical stimulation were unaffected in contralateral paws, sham-operated mice or in naive untreated mice (Fig. 1a). At this time point, Epac1 mRNA levels in dorsal root ganglia (DRG) innervating the ipsilateral paw increased in comparison with DRG innervating the contralateral paw, from sham-operated animals, or from untreated mice by ~1.8-fold (Fig. 1b). Epac2 mRNA expression levels in DRG innervating the ipsilateral or contralateral paw were similar to Epac2 expression levels in DRG from sham-operated animals or naive untreated animals (Fig. 1c). The increase in Epac1 mRNA levels in the DRG innervating the ipsilateral paw was also observed at the protein level (Fig. 1d).

Epac1-dependent allodynia in neuropathic pain. Next we investigated whether Epac1 has a role in the development of allodynia in an L5 SNT neuropathic pain model. Epac1 protein levels were absent in DRG of *Epac1* −/− mice, while Epac1 protein levels were reduced by ~50% in *Epac1* +/− mice compared with wild-type (WT) mice (Fig. 1e). In control WT mice, spinal nerve transaction (SNT) induced mechanical allodynia that was present from day 1 after the operation and had fully developed in ~6 days. In mice completely deficient for Epac1 ($n=13$), SNT-induced allodynia was greatly attenuated compared with WT mice ($P<0.001$; $n=10$; two-way analysis of variance) or *Epac1* +/− mice ($P<0.001$; $n=10$; two-way analysis of variance) from day 1 (Fig. 1f). The magnitude of allodynia in *Epac1* +/− mice was also reduced compared with WT littermates ($P<0.05$; $n=10$; two-way analysis of variance) using repeated measures analysis (Fig. 1f). Overall these data indicate Epac1 is required for the development of allodynia in a mouse model of chronic neuropathic pain.

Epac signalling enhances sensory neuron mechanotransduction. Sensory neurons are intrinsically mechanosensitive and different types of mechanically gated current can be identified in the cell bodies of sensory neurons *in vitro*[15,16]. Neurons associated with detection of touch express low threshold rapidly adapting (RA) mechanically gated currents[2]. We asked whether activation of the cAMP-sensor Epac leads to changes in mechanically evoked RA currents in DRG neurons? Large diameter neurons (>35 μm) with fast action potentials (width of action potential <1 ms) were mechanically distended[17]. Application of the Epac-selective cAMP analogue 8-pCPT shifted the stimulus response curves of mechanically evoked RA currents to the left, resulting in increased currents in response to mechanical stimuli (~2-fold increase in inward current at a stimulus intensity of 12 μm) (Fig. 2a,d). 8-pCPT time dependently enhanced mechanically activated peak currents evoked by a ~12.5-μm distension that plateaued after ~15 min (Fig. 2b,d). Finally, 15 min after application of 8-pCPT the threshold of activation of RA currents was reduced by ~24% (Fig. 2c). Application of vehicle did not have any effect on mechanically evoked current sizes (Fig. 2).

Characterization of human Piezo2. DRG neurons in culture express at least three types of cation currents evoked by mechanical stimulation[16–18]. Piezo2 is expressed in mouse sensory neurons[4], and Piezo2 short interfering RNA application to sensory neuron cultures results in a ~75% loss of neurons expressing mechanically evoked RA currents[4]. As the Epac-specific cAMP analogue sensitized mechanically evoked RA currents, we first cloned human PIEZO2 (hPiezo2) cDNA into a mammalian expression vector, transfected it into HEK293 cells and characterized its biophysical properties by whole-cell voltage clamp. hPiezo2 currents activated within ~1 ms of the mechanical stimulus and were weakly outwardly rectifying (Fig. 3a) with a reversal potential of 9.7 ± 1.6 mV ($n=7$). hPiezo2 currents showed rapid adaptation to the mechanical stimulus which was voltage dependent, being 7-fold faster at negative holding voltages than positive holding voltages (V_{hold} −80 mV, Tau = 4.4 ± 0.8 ms; V_{hold} +80 mV, Tau = 29.4 ± 3.5 ms; $n=7$; $P<0.001$; *t*-test). Mechanically stimulating hPiezo2-expressing HEK293 cells at a rate of 1 Hz resulted in a rapid decay in the size of the mechanically evoked current (Supplementary Fig. S1a,b), similar to native rapidly adapting (RA) currents in DRG[19]. We next investigated the pharmacology of hPiezo2 (Fig. 3b–d). Acute bath addition of FM1-43, a permeant inhibitor of rapidly adapting mechanosensitive channels in sensory neurons[20], inhibited hPiezo2 currents (Fig. 3b–d). By contrast preincubation with dihydrostreptomycin, a blocker of the cochlear mechanotransducer channel[21], had no effect on either the magnitude or threshold of hPiezo2 currents (Fig. 3e,f).

Further characterization of hPiezo2 showed that mechanically evoked peak currents were directly proportional to probe velocity (Supplementary Fig. S1c,d), with decreased probe velocity resulting in smaller mechanically evoked currents. The

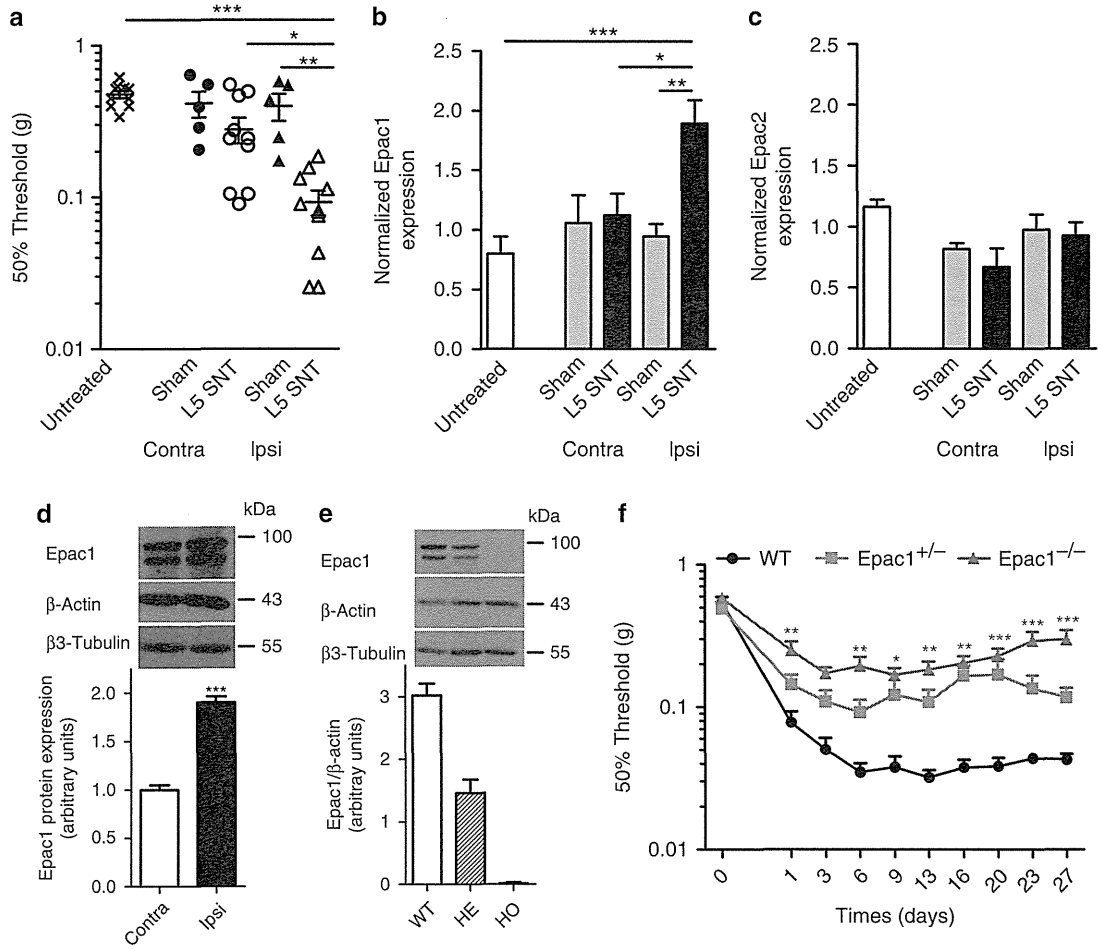

Figure 1 | DRG Epac1 expression is increased in and required for L5 spinal nerve transaction-induced allodynia. (**a**) The sensitivity to mechanical stimulation was determined in sham-operated mice ($n=5$), naive controls ($n=10$) or mice subjected to unilateral L5 SNT 4 weeks after surgery ($n=10$). Line with error bars represent mean ± s.e.m. (**b**) Epac1 or (**c**) Epac2 mRNA levels in DRGs innervating the contralateral (contra) or ipsilateral (ipsi) side of sham-operated, naive controls and L5 SNL mice 4 weeks after surgery. Epac1/2 mRNA expression levels were corrected for GAPDH and β-actin mRNA expression levels. (**d**) Epac1 protein expression levels in ipsilateral (affected) and contralateral (unaffected) DRGs of mice subjected to unilateral L5 SNT 4 weeks after surgery. β-Actin and the neuron-specific β3-tubulin was used as loading control. (**e**) Epac1 protein expression in DRGs of WT ($n=6$), Epac1+/− (HE, $n=4$) and Epac1−/− (HO, $n=4$) mice. (**f**) The sensitivity to mechanical stimulation was determined in wild-type ($n=10$), *Epac1*+/− ($n=10$) and *Epac1*−/− ($n=13$) mice subjected to unilateral L5 SNT. Repeated measures one-way analysis of variance (ANOVA) showed a significant genotype effect $F(2,30)=25{,}935$, $P<0.001$. Bonferoni *post hoc* analysis showed a significant effect between *Epac*−/− and WT ($P<0.001$); *Epac1*−/− and *Epac1*+/− ($P<0.001$); and *Epac1*+/− and WT ($P<0.05$). All data are expressed as mean ± s.e.m. (**a–c**) Data are analysed by ANOVA followed by the Bonferroni *post hoc* test. (**d**) Data are analysed using *t*-test. *$P<0.05$, **$P<0.01$, ***$P<00.1$.

biophysical properties of hPiezo2 are similar to those described for mouse Piezo2 and endogenous RA mechanosensitive currents expressed in large and small diameter DRG neurons[4,16,18]. Cytoskeletal elements have previously been shown to be essential for normal mechanotransduction in sensory neurons[16,22]. Preincubation of HEK293 cells overexpressing hPiezo2 with the actin depolymerizing agent latrunculin A strongly shifted the stimulus–response curve to the right resulting in a reduction in mechanical sensitivity of hPiezo2 (Supplementary Fig. S1e). Latrunculin A increased the threshold for activation ~5-fold (control: 2.4 ± 0.5 μm; lantruculin: 12.3 ± 1.2 μm, $P<0.001$; $n=6$–7; *t*-test). The microtubule depolymerizing agent colchicine reduced hPiezo2 peak currents in response to mechanical stimuli ≥7 μm (Supplementary Fig. S1f). However, no shift in the stimulus–response curve or change in mechanical threshold (control: 3.3 ± 0.5 μm; colchicine: 4.2 ± 0.4 μm; $P=0.15$; $n=16$; *t*-test) was observed. These findings indicate that the actin and tubulin cytoskeletons regulate hPiezo2 via distinct mechanisms.

Epac1 signalling enhances Piezo2-mediated mechanotransduction. As Epac signalling sensitizes mechanically evoked RA currents, we also tested effects on Piezo2-mediated mechanically evoked currents. We used HEK293a cells expressing Piezo2 and Epac1 or Epac2 (HEK293a cells express very low levels of Epac1/2) and mechanically distended these cells. Coexpression of Epac1 with Piezo2 in HEK293 cells did not change the stimulus–response curve compared with expression of Piezo2 alone (Fig. 4a). However, the addition of Epac-selective 8-pCPT to cells expressing Piezo2 and Epac1 strongly shifted the stimulus–response curve to the left. At a distension of ~8 μm, currents increased by ~2.5-fold (Fig. 4a,e). Coexpression of Epac2 with Piezo2 or application of 8-pCPT to cells expressing

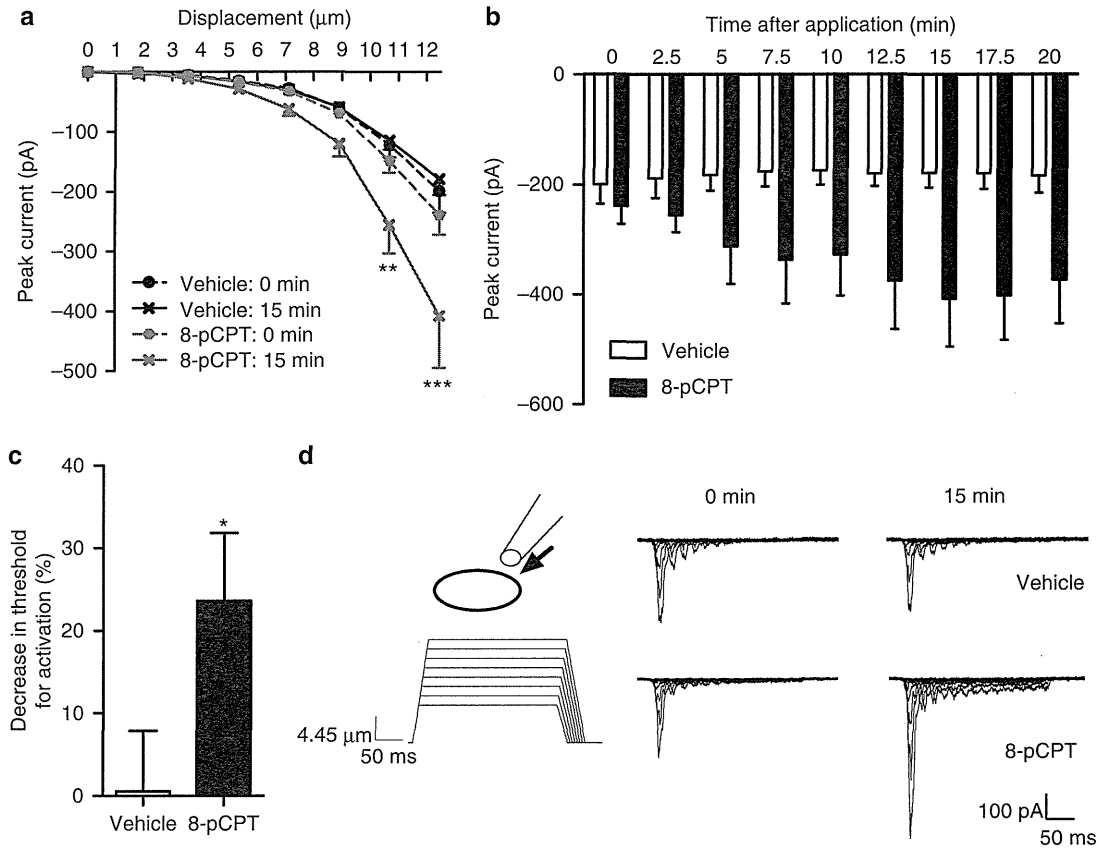

Figure 2 | 8-pCPT enhances rapidly adapting mechanically evoked currents in large diameter sensory neurons. (**a**) Stimulus-response curve of rapidly adapting currents evoked by mechanical stimulation before and 15 min after 8-pCPT or vehicle administration (vehicle, $n=13$; 8-pCPT, $n=17$). (**b**) Time course of peak currents evoked by a ~12.5-μm membrane deflection after administration of 8-pCPT into the bath solution. Repeated measures one-way analysis of variance: time, $P<0.05$; treatment, $P>.05$; interaction: $P<0.01$ ($n=14$). (**c**) Threshold of activation was determined as mechanical stimulus that elicited a current >20 pA. The decrease in threshold of activation after 8-pCPT was calculated as percentage of baseline thresholds. (**d**) Representative example of whole-cell voltage clamp traces from a large diameter mouse DRG neuron with a narrow action potential width in response to increasing membrane deformation (holding potential −60 mV) before and after 8-pCPT or vehicle administration. All data are expressed as mean ± s.e.m. (**a–b**) Data were analysed using two-way analysis of variance followed by the Bonferroni *post hoc* test. (**d**) Data are analysed by *t*-test. $^*P<0.05$, $^{**}P<0.01$, $^{***}P<0.001$.

Piezo2 + Epac2 or Piezo2 alone did not change the stimulus–response curve (Fig. 4b). In Epac1 expressing cells, 8-pCPT also increased the maximal mechanically evoked inward current before whole-cell configuration was lost because of the strength of the mechanical stimulus and reduced the threshold of activation, whereas Epac2 had no effect on either parameter (Fig. 4c,d). In cells expressing hPiezo1 and Epac1, 8-pCPT-induced activation of Epac1 also shifted the stimulus response of mechanically evoked Piezo1 currents to the left and decreased thresholds of activation, whereas no effect was seen when Epac2 was coexpressed with hPiezo1 (Supplementary Fig. S2). Overall these data indicate that Epac1 but not Epac2 activation results in sensitization of mechanically evoked Piezo-dependent currents. We further tested whether activation of other signalling molecules known to be involved in the development of mechanical hypersensitivity such as PKA, protein kinase C (PKC) and Ca^{2+} sensitize Piezo2 currents. Increasing cytosolic Ca^{2+} from 50 nM to 1 μM in Piezo2 expressing HEK293 cells resulted in sensitization of the mechanically evoked current (Supplementary Fig. S3a,b) and a reduction in threshold for channel activation (Supplementary Fig. S3c). Elevating cytosolic calcium also produced a marked slowing of adaptation to the static mechanical stimulus at cell displacements ≥4 μm (Supplementary Fig. 3d). In contrast, activation of PKC by pre-incubation with the phorbol derivative PMA had no effect on hPiezo2 channel activity or threshold (Supplementary Fig. S3e,f). Similarly, activation of PKA by preincubation with 6-Bnz-cAMP, a selective agonist of PKA, which does not activate Epac, had no significant effect on the stimulus–response curve (Supplementary Fig. S3g,h).

Epac activation causes long-lasting mechanical allodynia. 8-pCPT has been shown to cause increased sensitivity to noxious mechanical stimuli (hyperalgesia)[23]. Activation of the cAMP-sensor PKA, induces hyperalgesia through effects on excitability, but not through sensitizing mechanotransduction[1]. We tested whether selective activation of Epac increased sensitivity to touch and compared this with the development of mechanical hypersensitivity induced by a PKA-selective cAMP analogue (6-Bnz-cAMP). Intraplantar injection of either 6-Bnz-cAMP or 8-pCPT dose-dependently (12.5 pmol per paw–12.5 nmol per paw) induced mechanical hypersensitivity that increased in magnitude and duration with increasing doses (Fig. 5a,b). At every dose tested, the magnitude of 6-Bnz-cAMP and 8-pCPT-induced mechanical hypersensitivity was statistically indistinguishable

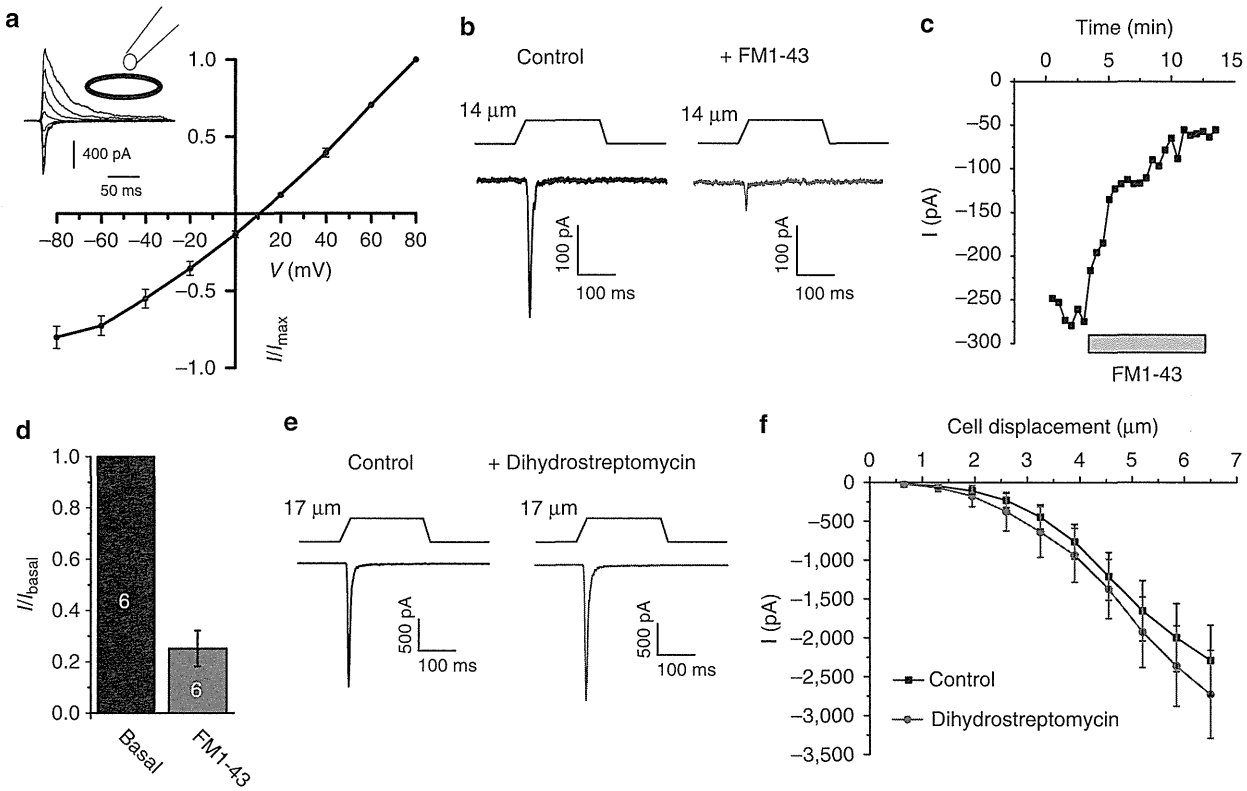

Figure 3 | Biophysical characterization of hPiezo2. (**a**) Mean current voltage relationship of hPiezo2 expressed in HEK293 cells in response to a 4 µm displacements of the membrane ($n=7$). hPiezo2 currents were recorded using the perforated configuration of the whole-cell patch clamp technique. Inset shows example current trace at the different holding voltages. (**b**) Typical steady-state current traces at a holding potential of −70 mV recorded before (control) and after addition of FM1-43 (15 µM) to the bathing solution. Mechanical probe displacement is shown inset (positioned 11 µm from cell). (**c**) Example time course of FM1-43 inhibition showing peak mechanically evoked current in response to a 3-µm membrane displacement. Time at which FM1-43 was added to the bathing solution is indicated by the grey bar. (**d**) Mean fractional inhibition of hPiezo2 currents. Number of experiments is indicated within bars. (**e**) Typical current traces in response to a 6-µm membrane displacement after 15 min preincubation in vehicle (control) or dihydrostreptomycin (10 µM). Mechanical probe displacement is shown inset (positioned 11 µm from cell). (**f**) Mean peak mechanically evoked currents. Data are expressed as mean ± s.e.m.

(Fig. 5a). Importantly, however, 8-pCPT-induced mechanical hypersensitivity lasted significantly longer than 6-Bnz-cAMP-induced mechanical hypersensitivity (Fig. 5b,c). At the highest dose tested (12.5 nmol per paw), 8-pCPT-induced sensitization lasted ~3 days while 6-Bnz-cAMP-induced mechanical hypersensitivity only lasted ~1 day (Fig. 5c).

8-pCPT-induced mechanical sensitization was dependent on DRG Epac1 as intrathecal Epac1 antisense oligodeoxynucleotides (ODNs) administration reduced DRG protein levels for Epac1 by ~44% and almost completely prevented development of mechanical sensitization induced by 8-pCPT (Fig. 5d,e). Epac1 antisense ODN treatment did not affect baseline thresholds to von Frey filaments (Fig. 5e). The Epac1 antisense ODN strategy was confirmed by using Epac1 knockout mice. 8-pCPT-induced mechanical allodynia was prevented in *Epac1*−/− mice (Fig. 5f; $P<0.001$; $n=8$–12; two-way analysis of variance) and *Epac1*+/− mice (Fig. 5f; $P<0.05$; $n=8$–12; two-way analysis of variance). *Epac*+/− mice did not statistically differ from *Epac1*−/− mice. 6-Bnz-cAMP-induced mechanical hypersensitivity was indistinguishable between WT, *Epac1*−/− and *Epac1*+/− mice (Fig. 5g). Thus, the activation of cAMP-sensor Epac1 leads to sensitization that is longer in duration (3–4 days) than PKA-mediated hypersensitivity (<1 day). Importantly, Epac1 antisense-treated and genetically modified mice with low Epac1 protein levels indicate that partial reduction of Epac1 induces large behavioural effects.

To determine whether sensitization of mechanotransducing channels underlies 8-pCPT-induced mechanical allodynia, we used intraplantar FM1-43 that blocks mechanically activated currents in sensory neurons and Piezo2 currents (Fig. 3d)[20]. Intraplantar FM1-43 almost completely reversed 8-pCPT-induced allodynia (Fig. 5h). As shown before[20], injection of FM1-43 doubled the threshold to mechanical stimulation in naive control mice (Fig. 5h). Thus, Epac1 activation causes a long-lasting increase in sensitivity to touch that is mediated through mechanosensitive channels *in vivo*.

Epac signalling enhances wide dynamic range responses to mechanical stimuli. Lamina V wide dynamic range (WDR) neurons in the dorsal horn respond to all sensory modalities. Extracellular recording from rat WDR neurons in response to mechanical input to the receptive field showed that 8-pCPT enhanced WDR neuron firing in response to mechanical stimuli applied to the hind paw that was ≤26 g (Fig. 6a). In contrast, 6-Bnz-cAMP only enhanced WDR neuron firing in response to mechanical stimuli applied to the receptive field (hind paw) that were larger than 15 g (Fig. 6b). Intraplantar injection of saline did

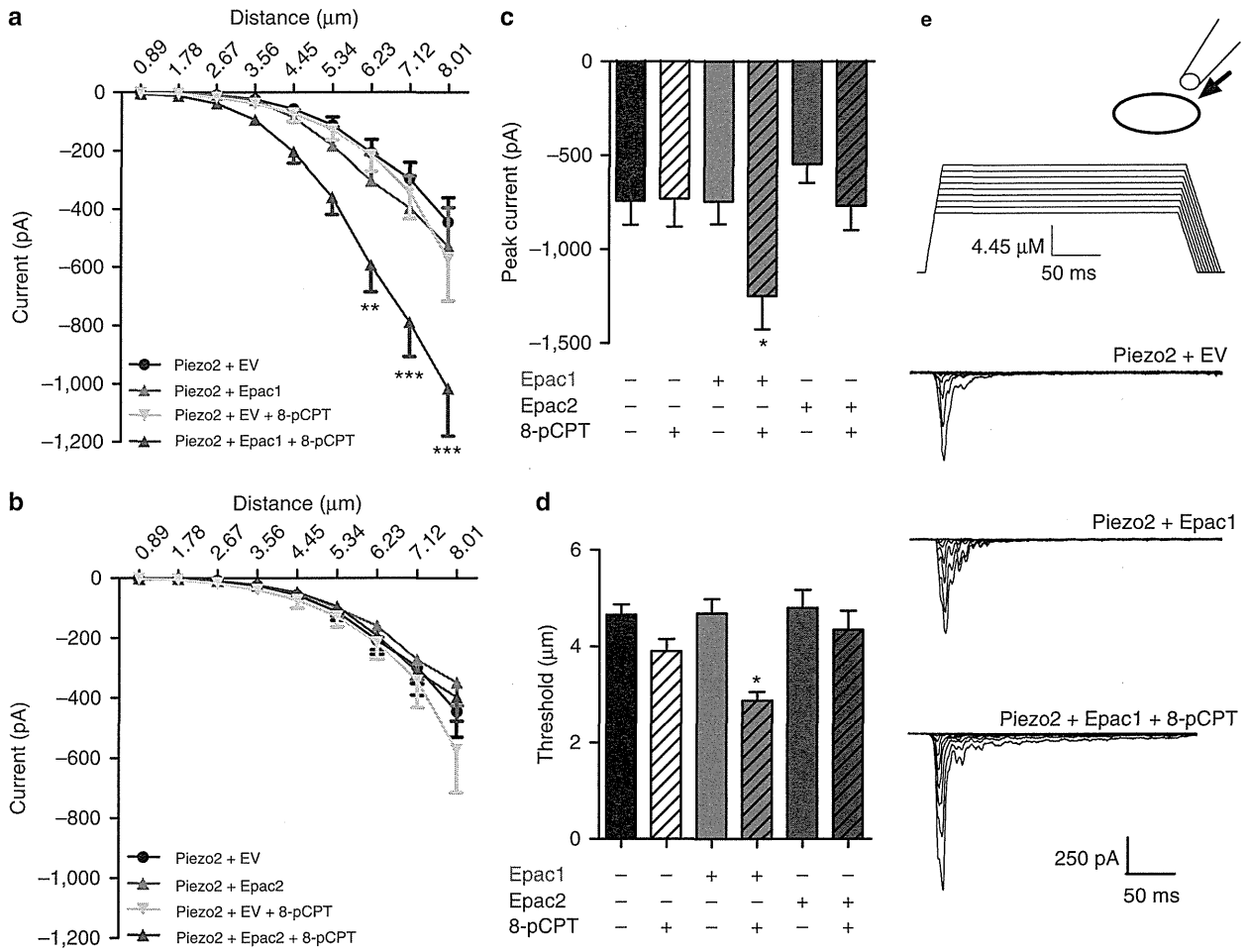

Figure 4 | Activation of Epac1 but not Epac2 sensitizes mechanically evoked Piezo2 currents. HEK293a cells were transfected with constructs encoding Piezo2 + empty pcDNA3 (EV, + 8-pCPT, $n = 21$; + vehicle, $n = 38$), and (**a**) Piezo2 + Epac1-YFP (+ 8-pCPT, $n = 26$; + vehicle, $n = 30$), or (**b**) Piezo2 + Epac2-YFP (+ 8-pCPT, $n = 17$, + vehicle, $n = 23$). 8-pCPT (specific Epac activator) or vehicle was added and cells were voltage clamped at − 70 mV in whole-cell configuration. (**a/b**) Mechanically evoked currents were elicited by increasing displacement of the cell membrane in ~0.9 μm increments. (**c**) Peak current elicited by the largest mechanical stimulus before whole-cell configuration was lost. (**d**) Threshold of activation was determined as the mechanical stimulus that elicited a current > 20 pA. (**e**) Exemplar traces of currents in response to increasing membrane deformation of HEK293a cells expressing Piezo2 + EV, Piezo2 + Epac1 and Piezo2 + Epac1 + 8-pCPT. All data are expressed as mean ± s.e.m. (**a-b**) Data were analysed using two-way analysis of variance followed by the Bonferroni *post hoc* test. *$P < 0.05$, **$P < 0.01$, ***$P < 0.001$. In **c** and **d** '*' indicates significant difference compared with all other groups analysed by one-way analysis of variance followed by the Bonferroni *post hoc* test.

not change WDR neuron firing responses evoked by any mechanical stimuli (Fig. 6c).

The enhanced responses to mechanical stimuli could be mediated via changes in electrical excitability or at the level of mechanotransduction. Intraplantar 8-pCPT administration did not change WDR responses evoked by electrical activation of Aβ, Aδ or C fibres (Fig. 6d). Moreover, no changes in input, post-discharge or wind-up were observed (Fig. 6d). Both afferent electrical and central excitability are unaffected by 8-pCPT in line with our observation that 8-pCPT-induced allodynia is unaffected in mice deficient for DRG expression of voltage-gated sodium channels Nav1.7, Nav1.8 or Nav1.9 (Supplementary Fig. S4). Intraplantar injection of 6-Bnz-cAMP activates PKA and enhanced C-fibre-evoked WDR responses as well as input (a measure of afferent drive) but did not change electrically evoked Aβ- or Aδ-mediated WDR responses (Fig. 6e). Moreover post-discharge or wind-up were not changed by 6-Bnz-cAMP (Fig. 6e). Intraplantar vehicle injection did not induce any changes in electrically evoked WDR responses (Fig. 6f). These data indicate that 8-pCPT enhances responses to mechanical stimuli independent of changes in electrical excitability.

Epac1-mediated allodynia is Nav1.8 + nociceptor independent. Nav1.8 + sensory neurons comprise 85% of nociceptors and are essential for detecting noxious mechanical stimuli as well as for development of inflammatory hyperalgesia, but not neuropathic pain[24]. To test whether Nav1.8 + sensory neurons are required for 8-pCPT-induced mechanical allodynia, we used diphtheria toxin to kill these sensory neurons (*Nav1.8-DTA*[24]). As reported[24], baseline sensitivity to touch was similar in WT and Nav1.8-DTA mice (Fig. 7a). Importantly, the course of 8-pCPT-induced mechanical allodynia in mice in which Nav1.8 nociceptors were ablated was indistinguishable from control littermates (Fig. 7a). The absence of an effect of Nav1.8 nociceptor depletion on 8-pCPT-induced mechanical allodynia was independent of the dose of 8-pCPT; at any dose of 8-pCPT tested (12.5 pmol per paw–12.5 nmol per paw) mice showed no

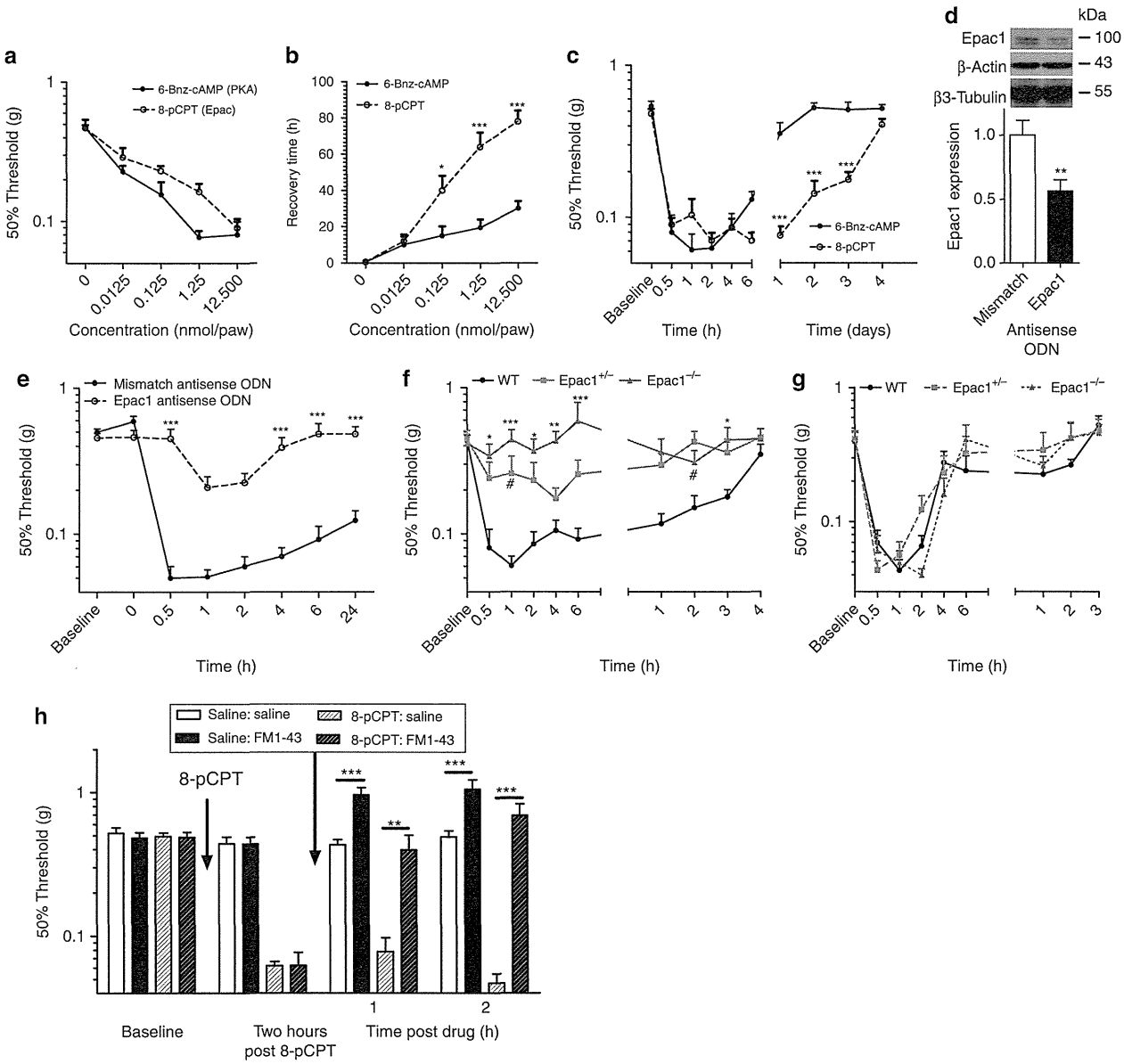

Figure 5 | The selective Epac activator 8-pCPT induces an Epac1-dependent long-lasting allodynia *in vivo*. Different doses of 8-pCPT (specific Epac activator; $n=4-8$) or 6-Bnz-cAMP (specific PKA activator; $n=4-8$) were injected intraplantarly and (**a**) 50% threshold to von Frey was determined 30 min after administration of drug. (**b**) Duration of 6-Bnz-cAMP or 8-pCPT-induced mechanical allodynia determined as the earliest time point in which 50% threshold is equal or higher than the average baseline 50% threshold ± 2x standard deviation ($n=4$–8). Time course of (**c**) mechanical hypersensitivity after intraplantar injection of 8-pCPT or 6-Bnz-cAMP (12.5 nmol per paw, $n=8$). (**d-e**) Epac1 antisense or mismatch antisense ODN were administered intrathecally once every two days for three times. (**d**) Two days after the last injection L2-L5 DRG Epac1 protein levels were determined by western Blot ($n=4$). (**e**) Time course of 8-pCPT-induced allodynia using von Frey in antisense ODN-treated animals ($n=8$). Repeated measures one-way analysis of variance: ODN treatment: $P<0.001$; time: $P<0.001$; interaction: $P<0.001$. (**f**) Time course of intraplantar 8-pCPT-induced allodynia (12.5 nmol per paw) in WT ($n=12$), *Epac1*+/− ($n=8$), and *Epac1*−/− ($n=8$) mice. Statistical analysis showed a genotype effect ($F(2, 25)=13{,}053$, $P<0.01$) and *post hoc* analysis shows that *Epac1*−/− ($P<0.001$) as well as *Epac1*+/− ($P<0.05$) significantly differed from WT mice. (**g**) Time course of intraplantar 6-Bnz-cAMP-induced mechanical allodynia (12.5 nmol per paw) in WT ($n=8$), *Epac1*+/− ($n=6$), *Epac1*−/− ($n=8$) mice. (**h**) Mice received intraplantar injection of 8-pCPT or vehicle and sensitivity of the mechanical stimulation was determined after 2 h. At this time point mice received an injection of FM1-43, or vehicle and threshold to mechanical stimulation was determined 1 and 2 h after injection. Data are expressed as mean ± s.e.m. Data were analysed using two-way analysis of variance followed by the Bonferroni *post hoc* test. (**d**) Data are analysed by *t*-test $^*P<0.05$, $^{**}P<0.01$, $^{***}P<0.001$. In f '#' indicates $P<0.05$ compared to WT mice.

notable difference in magnitude (Fig. 7b) or duration (Fig. 7c) of mechanical allodynia in *Nav1.8-DTA* mice compared with control littermates.

In contrast to nociceptor-independent mechanical allodynia induced by Epac activation, we found that PKA activation could sensitize mechanosensation through effects on Nav1.8+ nociceptors. Increasing doses of 6-Bnz-cAMP induced mechanical hypersensitivity that increased in magnitude and duration. The magnitude as well as the duration of 6-Bnz-cAMP-induced mechanical hypersensitivity was severely reduced in

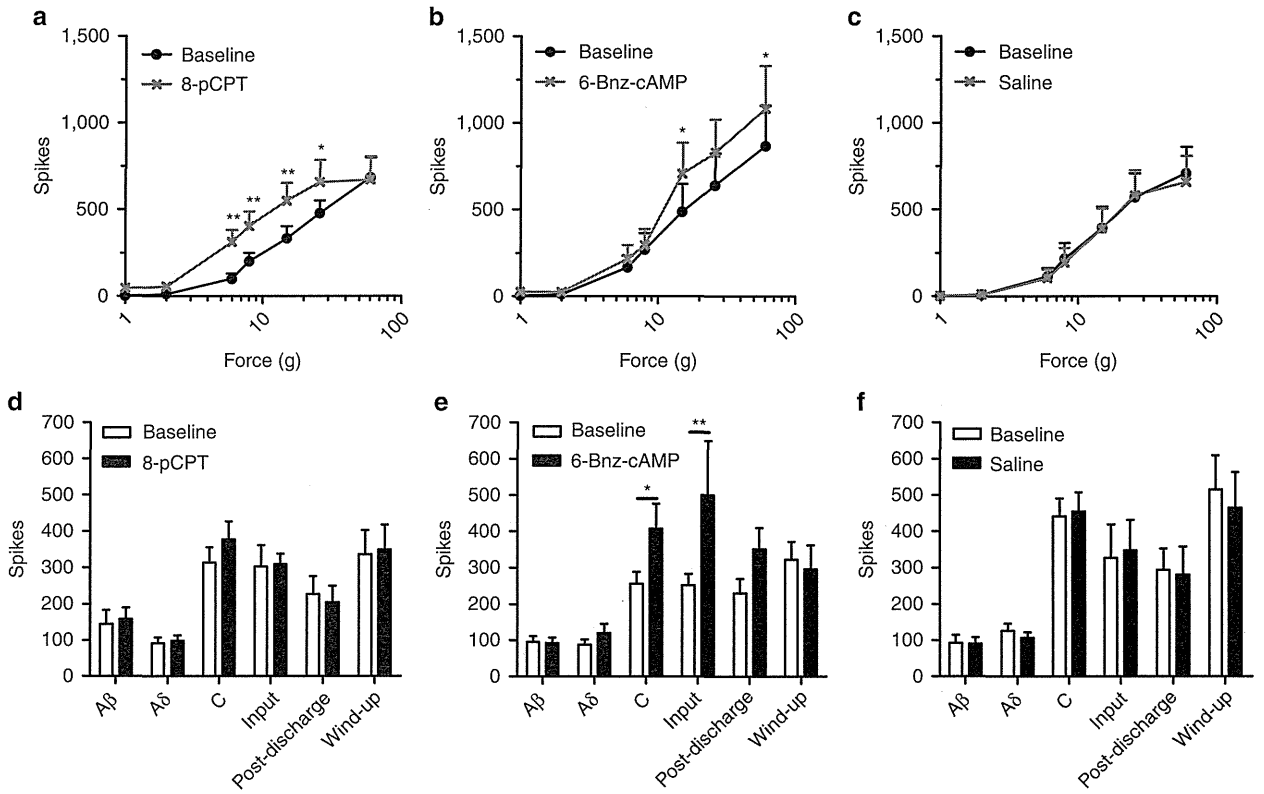

Figure 6 | *In vivo* electrophysiology of WDR neuron firing response after intraplantar 8-pCPT or 6-Bnz-cAMP. Evoked responses to von Frey filaments before and after administration of (**a**) 8-pCPT ($n=8$), (**b**) 6-Bnz-cAMP ($n=8$), or (**c**) saline ($n=7$). 8-pCPT shifted the stimulus-response curve to the left and enhanced responses to innocuous von Frey, while 6-Bnz-cAMP only enhanced response of von Frey >16 g. Responses to transcutaneous electrical stimulation of the receptive field before and after intraplantar injection of (**d**) 8-pCPT ($n=8$), (**e**) 6-Bnz-cAMP ($n=9$), or (**f**) saline ($n=7$). Data are expressed as mean ± s.e.m. (**a–c**) Data were analysed using two-way analysis of variance followed by the Bonferroni *post hoc* test. (**d–f**) Data are analysed by t-test $^*P<0.05$, $^{**}P<0.01$.

Nav1.8-DTA mice at all doses tested (12.5 pmol per paw–12.5 nmol per paw) (Fig. 7d,e). These data indicate that the PKA-dependent 6-Bnz-cAMP-induced mechanical hypersensitivity was almost completely absent in nociceptor-depleted mice. The highest dose (12.5 nmol per paw) used induced some mechanical hypersensitivity in nociceptor-depleted mice, but was significantly less intense and shorter than in control littermates (Fig. 7f).

Piezo2 is required for 8-pCPT-induced allodynia. We tested whether sensitization of Piezo2 contributes to 8-pCPT-induced allodynia. Intrathecal injection of antisense oligonucleotides (ODN) results in their concentration in DRG neurons, where RNA–DNA hybrids are degraded by RNase H; this approach to downregulating gene expression has been used in a variety of studies.[25] However, possible effects of antisense ODN in other cells within the spinal cord and DRG cannot be excluded. Intrathecal injection of a mixture of three different Piezo2 antisense ODN reduced Piezo2 mRNA expression in L2-L5 DRG by ~26%, 2 days after the last injection of antisense ODN (Fig. 7g). The reduction of DRG Piezo2 mRNA expression was associated with an increase in baseline thresholds to mechanical stimulation (Fig. 7h). 8-pCPT-induced mechanical allodynia was attenuated in Piezo2 antisense ODN-treated animals compared with mismatch ODN-treated mice (Fig. 7h). The partial reduction in Piezo2 mRNA is consistent with the behavioural effect of Piezo2 antisense treatment on 8-pCPT-induced allodynia.

Role of Piezo2 in touch sensation and allodynia. As Piezo2 antisense ODN treatment reduced Epac-mediated allodynia, we examined whether Piezo2 contributes to neuropathy induced allodynia and whether Piezo2 is involved in touch perception. Piezo2 antisense ODN mixture reduced Piezo2 mRNA expression in L2-L6 DRG by ~35% as measured 1 day after the last injection of Piezo2 antisense ODN, with no effect on Piezo1 levels (Fig. 7i). Piezo2 antisense ODN did not affect motor behaviour (Supplementary Fig. S5a). However, the reduction of Piezo2 mRNA expression was associated with an increase in 50% threshold to light mechanical stimulation to the hind paw (Fig. 7j). By contrast, responses to noxious mechanical stimulation or noxious heat were similar to mismatched control ODN-treated mice (Supplementary Fig. S5b,c).

To investigate the role of Piezo2 in neuropathy-induced allodynia, a unilateral L5 nerve transaction (L5 SNT) or a sciatic nerve ligation (chronic constriction injury (CCI)) was performed in mice to induce neuropathic pain. In both models mice developed mechanical allodynia in the ipsilateral paw, while mechanical thresholds to touch in the contralateral paw were unaffected (Fig. 8a–e). In the L5 SNT model, mice were treated intrathecally with Piezo2 antisense ODN starting at day 15. Piezo2 antisense treatment significantly attenuated L5 SNT-induced allodynia compared with mismatch-treated mice (Fig. 8a). Piezo2 antisense ODN treatment also increased thresholds to touch compared with mismatch antisense-treated mice at the unaffected contralateral paw (Fig. 8a). In the CCI model of neuropathic pain, multiple intrathecal Piezo2 antisense injections also significantly

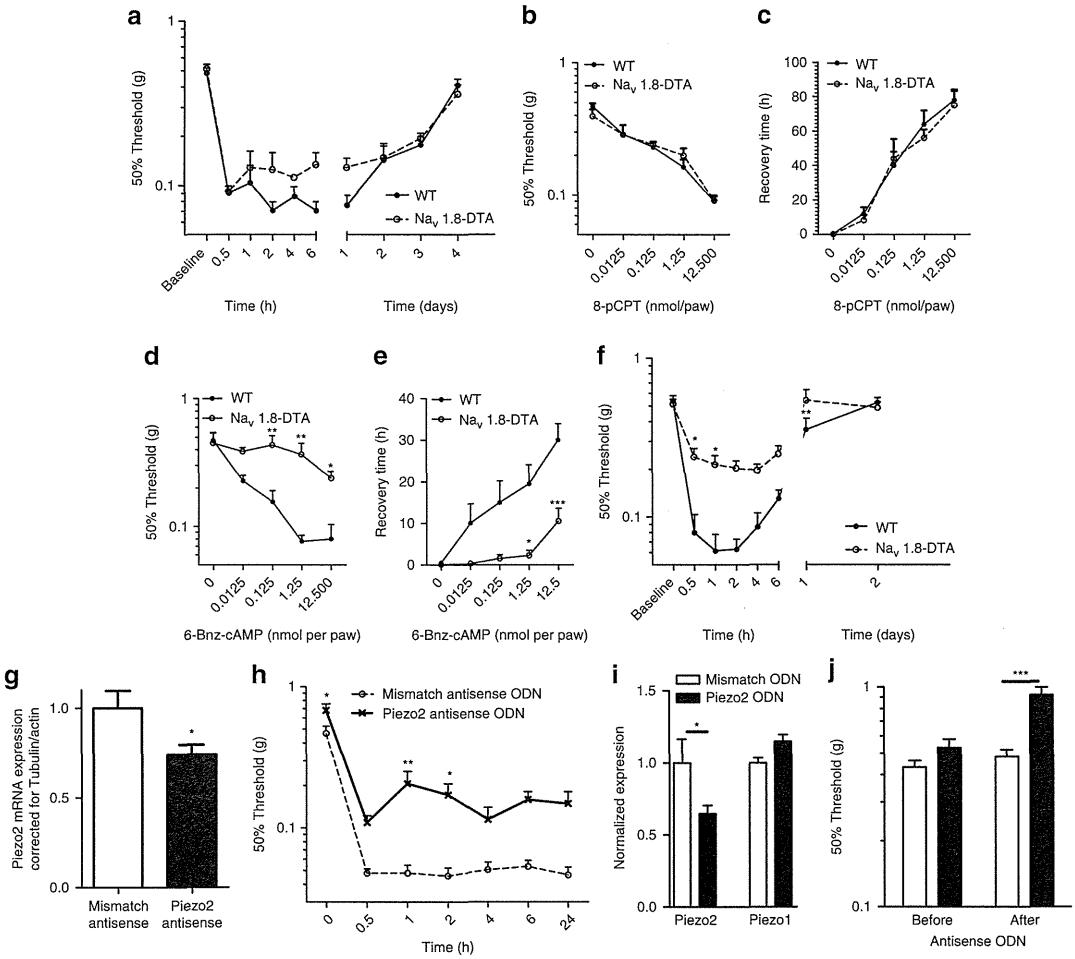

Figure 7 | Epac signalling-mediated allodynia is Piezo2 dependent and does not require Nav1.8 expressing nociceptors. WT and nociceptor-depleted mice *(Nav1.8-DTA)* received an intraplantar injection of 8-pCPT (12.5 nmol per paw) and time course of (**a**) allodynia ($n=8$) was determined. WT and *Nav1.8-DTA* mice received different doses of 8-pCPT (**b**, $n=4$–8) or 6-Bnz-cAMP (**d**, 6-Bnz-cAMP, $n=4$–8) and mechanical sensitivity was determined 5 h after intraplantar injection. Duration of 8-pCPT (**c**, $n=4$–8) or 6-Bnz-cAMP-induced (**e**, $n=4$–8) mechanical allodynia determined as the earliest time point in which the 50% threshold is equal or higher than the average baseline 50% threshold—2x standard deviation. (**f**) Time course of 6-Bnz-cAMP-induced (12.5 nmol per paw) allodynia ($n=8$). Repeated measures of allodynia: genotype: $P<0.001$, time: $P<0.001$, interaction: $P<0.05$. (**g**–**h**) Piezo2 or mismatch antisense ODNs were administered intrathecally 5, 3, 2, and 1 day before behavioural experiments. (**g**) Two days after the last injection L2-L5 DRG Piezo2 mRNA levels were determined by quantitative RT-PCR. (**h**) Time course of 8-pCPT-induced allodynia was determined using von Frey. (**i**) To verify role of Piezo2 in touch perception, one day after the last antisense ODN injection L2-L6 DRG Piezo1/2 mRNA expression levels were determined by quantitative RT-PCR. (**j**) Sensitivity to touch was determined using Von Frey filaments. Data are expressed as mean ± s.e.m. (**a**–**f**, **h**)Data were analysed using two-way analysis of variance followed by the Bonferroni *post hoc* test. (**g**,**i**) Data are analysed by *t*-test. (**j**) Data were analysed using one-way analysis of variance followed by the Bonferroni *post hoc* test. $^*P<0.05$, $^{**}P<0.01$, $^{***}P<0.001$.

attenuated CCI-induced mechanical allodynia (Fig. 8b). At the unaffected contralateral paw, Piezo2 antisense ODN treatment also increased thresholds to touch (Fig. 8b). Although Piezo2 antisense ODN increased mechanical thresholds both at the ipsi- and contralateral paw in both models of neuropathic pain, Piezo2 antisense ODN reduced the neuropathic pain-induced difference in mechanosensitivity between the contra and ipsilateral paw (Fig. 8c).

Twenty-four hours after the last Piezo2 antisense ODN injection, Piezo2 mRNA was reduced by more than 50% in both the ipsilateral and contralateral DRGs in both models of neuropathic pain (Fig. 8d,e). Piezo1 DRG mRNA expression levels were unaffected after Piezo2 antisense ODN treatment (Supplementary Fig. 6). These data show that transcription of Piezo1 and Piezo2 are unaffected by nerve damage as no difference between the ipsi and contralateral paw was observed.

Discussion

The molecular basis of touch and mechanical allodynia is poorly understood. Here, we show that activation of Epac1 contributes to the development of allodynia associated with neuropathic pain. Epac1 signalling produces allodynia involving Piezo2-mediated mechanotransduction in low threshold mechanosensitive sensory neurons independently of Nav1.8 + nociceptors. Epac1 signalling enhances mechanically evoked Piezo2-mediated currents in a heterologous expression system, as well as endogenous rapidly adapting mechanically gated currents in sensory neurons. We also

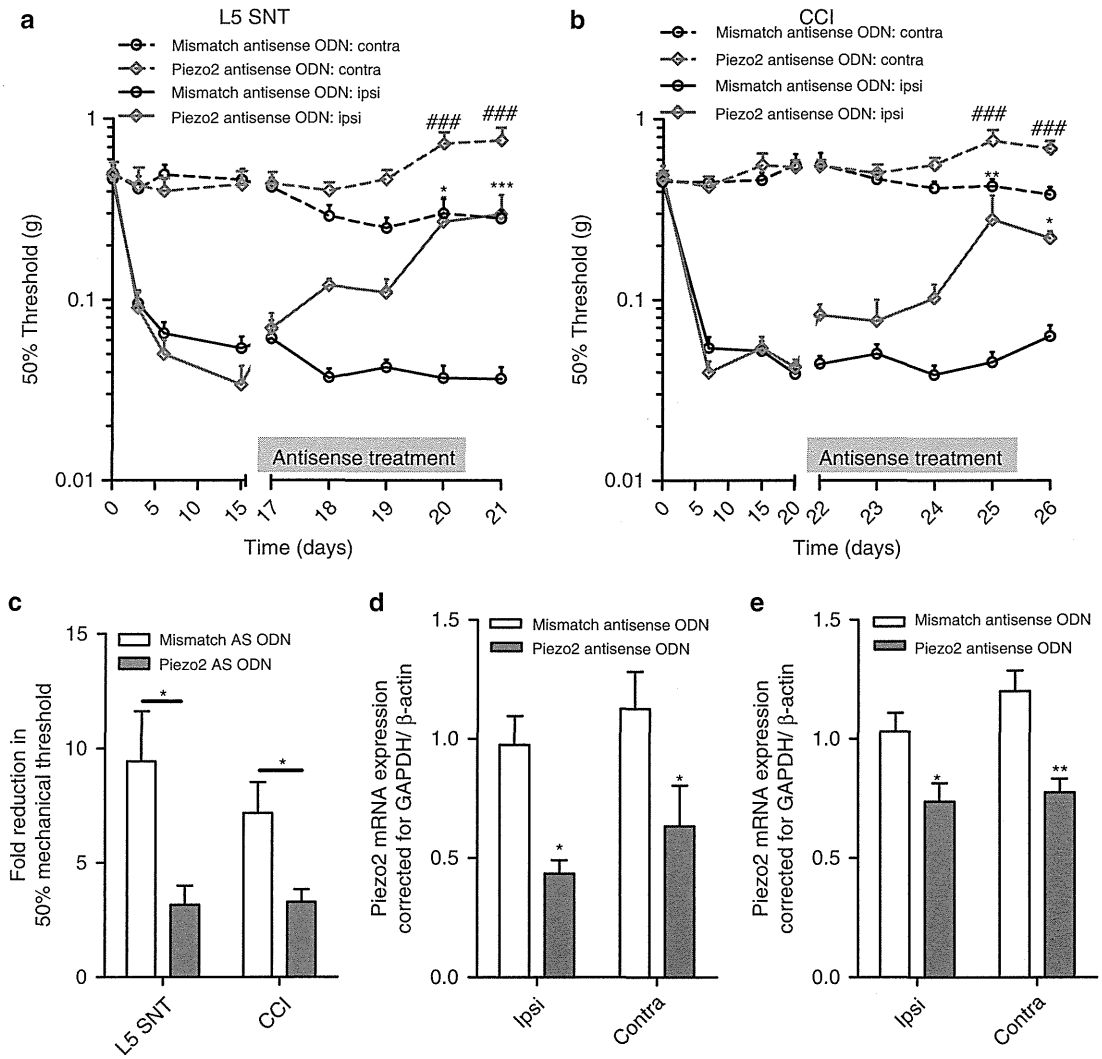

Figure 8 | Piezo2 is required for allodynia in two models of chronic neuropathic pain. Mice were subjected to a unilateral L5 spinal nerve transaction (L5 SNT; **a**) or to a unilateral chronic constriction injury of the sciatic nerve (CCI; **b**). The 50% threshold to von Frey was measured at the ipsilateral and contralateral paw. Piezo2 (L5 SNT, $n=5$; CCI, $n=6$) or mismatch antisense (L5 SNT, $n=9$; CCI, $n=10$) was administered after full development of allodynia (2-3 weeks after operation) as indicated by the grey bars. (**c**) Fold reduction of 50% threshold to von Frey of the ipsilateral paw compared the contralateral paw in both models of neuropathic pain at day 21 (L5 SNT; $n=5$-9) or 26 (CCI; $n=6$-10). Piezo2 mRNA expression in the ipsi- and contralateral DRG expression was measured 1 day after the last antisense ODN administration(**d**, L 5 SNT, $n=5$-9; **e**, CCI, $n=6$-10). Two-way one-way analysis of variance showed a significant overall reduction in Piezo2 mRNA $P<0.01$. Data are expressed as mean ± s.e.m. Data were analysed using two-way analysis of variance followed by the Bonferroni *post hoc* test. $^{*}P<0.05$, $^{**}P<0.001$, $^{***}P<0.001$. In **a** and **b** '###'indicate $P<0.001$ compared to the contralateral paw of mismatch antisense ODN treated mice.

show that Piezo2 is likely to have a role in the detection of light touch and the development of allodynia.

We found that Epac1 activation enhances mechanically evoked currents in low threshold mechanosensitive sensory neurons, many of which are associated with touch. Interestingly, this subset of sensory neurons lose their mechanically evoked currents after treatment with Piezo2 siRNA[4]. Mechanically evoked Piezo2 currents are enhanced upon Epac1 activation and *in vivo* activation of Epac1 produces a Piezo2-dependent allodynia that can be blocked by the permeant mechanosensory channel blocker FM1-43. PKA-mediated effects on mechanosensation do not involve mechanotransduction but act through sensitization of nociceptor electrical excitability[1], and activation of PKA does not enhance Piezo2 currents in HEK293 cells. Overall, Epac1 signalling appears to selectively enhance Piezo2-mediated mechanotransduction contributing to allodynia.

The contribution of cAMP signalling to sensitization of sensory neurons is well described. However, the role of the cAMP-sensor protein Epac1 in peripheral pain pathways is relatively unexplored. Intraplantar injection of the Epac agonist 8-pCPT has been shown to lead to a decrease in mechanical nociceptive thresholds in rats via a PKCε-dependent pathway[23]. We have found that activation of Epac1 leads to long-lasting allodynia, while activation of PKA induces a transient mechanical hypersensitivity linked to enhanced electrical excitability. The Epac1-mediated development of allodynia required a different subset of sensory neurons compared with those activated by PKA. PKA-mediated mechanical hyperalgesia requires

Nav1.8+ nociceptors, while Epac-mediated allodynia was independent of these sensory neurons. Earlier findings showed that 8-pCPT enhanced noxious mechanosensation in IB4+ sensory neurons,[23] that can be either Nav1.8+ or Nav1.8−. Interestingly, 8-pCPT-induced thermal hyperalgesia is almost completely absent in Nav1.8 nociceptor-depleted mice (Supplementary Fig. S7). Thus, these data indicate that Epac activation in non Nav1.8 expressing cells selectively leads to mechanical allodynia, while Epac activation in Nav1.8+ neurons causes thermal hyperalgesia or mechanical hyperalgesia in IB4+ neurons. Consistent with these observations, Nav1.8+ nociceptors are not required for the development of allodynia in a neuropathic pain model[24], and the development of allodynia is also attenuated in *Epac1*+/− and *Epac1*−/− mice in a neuropathic pain model. The sensory neuron subset-specific role of Epac1 signalling is also highlighted by the fact that reduction of an endogenous inhibitor of Epac1, G protein-coupled receptor kinase 2 in Nav1.8 expressing neurons, enhanced 8-pCPT-induced thermal hyperalgesia.[26] Finally, we have found that downstream signalling cascades activated by inflammatory mediators and linked to mechanical hyperalgesia rather than allodynia, such as PKC and PKA, do not alter Piezo2 currents. In contrast, increased intracellular calcium concentrations strongly potentiated hPiezo currents.

Although Aβ fibre-associated pain is little studied, Aβ nociceptors exist[27], and allodynia has been linked with Aβ sensory neuron activation[28]. It is also possible that besides the role of Epac1–Piezo2 in peripheral sensitization, other (spinal) processes induced by nerve damage link Aβ fibres to pain pathways.

The question arises whether Epac1 activation acts directly or indirectly on Piezo2. Epac signalling,has been shown to cause PKCε translocation to the cell membrane, and PLCε activation that could potentiate Piezo2-mediated currents through elevated intracellular calcium[29]. Further research to elucidate the mechanisms underlying Epac1-mediated Piezo sensitization and allodynia is required.

Characterization of human Piezo2 showed that this channel has similar properties to mouse Piezo2, already linked to rapidly adapting mechanically gated currents in DRG neurons. Consistent with this, antisense-mediated Piezo2 knockdown decreases mRNA expression and sensitivity to touch. This contrasts with the role of Piezo in *Drosophila*, which has no role in touch[30]. Intrathecal Piezo2 antisense ODN treatment attenuates mechanical allodynia induced by Epac1 activation or neuropathy.

In conclusion, these findings are the first to demonstrate a role for the cAMP-sensor Epac1 in mechanical allodynia in neuropathic pain and highlight Epac1 as a modulator of Piezo2, a mechanotransducer that we show here to be linked to mechanical allodynia and touch. These data suggest that the Epac1–Piezo2 axis is an important regulator of allodynia and is a potential therapeutic target for the treatment of neuropathic pain.

Methods

Animals. All behavioural tests were approved by the United Kingdom Home Office Animals (Scientific Procedures) Act 1986. *Epac1*+/−, *Epac1*−/− and their WT control littermates were from a C57BL/6 and CBA mixed background[31]. *Nav1.8*−/−, *Nav1.9*−/− C57Bl/6 and WT control littermates were used[32,33]. Nav1.7 deletion in all sensory neurons was accomplished by using heterozygous advillin-Cre/homozygous floxed Nav1.7 mice[34]. Ablation of Nav1.8 neurons was achieved by crossing heterozygous Nav1.8-Cre mice with homozygous eGFP-diphtheria toxin (DTA) mice[24]. For behavioural testing, mice aged 8–12 weeks were used. *In vivo* spinal cord electrophysiology was performed on Sprague-Dawley rats.

Measurement of mechanical allodynia and thermal hyperalgesia. The development of thermal hyperalgesia was measured with the Hargreave's apparatus[35]. Mechanical hyperalgesia was measured using von Frey hairs (Stoelting, Wood Dale, USA), and the 50% paw withdrawal threshold was calculated using the up-and-down method[36]. Noxious mechanical sensitivity was assessed using Randall Selitto apparatus[37]. Baseline withdrawal latencies or mechanical thresholds were averaged over at least three measurements before intraplantar injection of compounds or surgery. All experiments were performed in a blinded manner.

Drugs and preparation. Mice received an intraplantar injection of 2.5 µl of the Epac activator 8-(4-Chlorophenylthio)-2′-methyl-cAMP (8-pCPT; Biolog Life Science Institute, Bremen, Germany), or N6-Benzoyl-cAMP salt (6-Bnz-cAMP, Biolog Life Science Institute)[26]. As a control, a similar amount of vehicle was injected. FM1-43 (2 nmol µl^{-1}) was dissolved in saline and injected intraplantarly (2.5 µl) 2 h after 8-pCPT injection[20].

***In vivo* antisense ODN treatment.** Antisense ODNs[38] dissolved in saline (Epac1: 10 µg per 5 µl; Piezo2 mixture: 15 µg per 5 µl) were injected intrathecally[39]. Epac1 antisense ODN: mice were injected with Epac1 antisense ODN at 5, 3 and 1 days before injection of 8-pCPT. Piezo2 antisense ODN: mice were injected with Piezo2 antisense ODN at day 5, 3, 2 and 1 days before injection of 8-pCPT. During chronic neuropathic pain, Piezo2 antisense ODN were intrathecally injected daily. 24–48 h after the last injection DRGs were isolated. All antisense ODN had a phosphorothioate backbone.
The following ODN were used:
Epac1: 5′-AACTCTCCACCCTCTCCCA-3′; mismatch: 5′-ACATTCCACCCTC CTCCAC-3′
Piezo2: 5′-GTCCTTCCAGCCACATCTTCT-3′ + 5′-CCTTCTACCACCTCCT CCTC-3′ + 5′-ACCACCCGACCTCACAAGCA-3′; mismatch: 5′-TCCGTCTCG CACAACTCTCTT-3′ + 5′-CTTCTACCACTCCTCCCTCC-3′ + 5′-ACACCAC CCTCGCCAACGAA-3′.

Neuropathic pain models. A unilateral L5 nerve transaction (L5 SNT) was introduced in anaesthetized mice[40]. The L5 transverse process was removed using a blunt fine forceps and the left L5 spinal nerve was cut.
CCI was introduced to mice according to a modified protocol used for rats[41]. In anaesthetized mice, the left sciatic nerve was exposed at mid-thigh level and three loose ligatures were made around the nerve.

***In vivo* rat spinal cord electrophysiology.** Experiments were performed on anaesthetized male Sprague-Dawley rats (Central Biological Services, UCL), as previously described[42]. Saline, 8-pCPT or 6-Bnz-cAMP was administered into the receptive field of the cell (hind paw). The results were calculated as maximum change from the pre-drug control values for each response per neuron. See for full details Supplementary Methods.

Expression plasmids. The full-length hPiezo2 open reading frame was cloned into pcDNA3 (Invitrogen) in two sections to give the construct 'PIEZO2 in pcDNA3'. The 2,752 amino-acid PIEZO2 protein encoded by the construct is identical to NP_071351, except for containing SNPs rs7234309 (I) and rs3748428 (I). Finally, a polio IRES-eGFP fragment was PCR amplified from clone JC5 (ref. 45) and ligated into 'PIEZO2 in pcDNA3' to give the final construct 'PIEZO2-IRES-eGFP'. The coding sequence of the PIEZO2 construct has been sequenced entirely and has been submitted to GenBank under accession number JN790819. For Epac1/2 overexpression studies YFP-Epac1 and YFP-Epac2 were used[44].

Culture of DRG neurons. Adult mice DRG neurons were dissected out and subsequently digested in an enzyme mixture containing Ca^{2+}- and Mg^{2+}-free HBSS, 5 mM HEPES, 10 mM glucose, collagenase type XI (5 mg ml^{-1}) and dispase (10 mg ml^{-1}) for 1 h before mechanical trituration in DMEM + 10% heat-inactivated fetal bovine serum. Cells were centrifuged for 5 min at 800 r.p.m., resuspended in DMEM containing 4.5 g l^{-1} glucose, 4 mM L-glutamine, 110 mg l^{-1} sodium pyruvate, 10% fetal bovine serum, 1% penicillin–streptomycin (10,000 i.u. ml^{-1}), 1% glutamax, 125 ng ml^{-1} nerve growth factor, and plated on poly-L-lysine- (0.01 mg ml^{-1}) and laminin- (0.02 mg ml^{-1}) coated 35-mm dishes. Neurons were used 24 h after plating.

Cell culture. HEK293a cells were cultured in DMEM supplemented with 10% fetal calf serum (FCS). Plasmid DNA was transiently transfected into the cells using Lipofectamine 2000 (Invitrogen) in a ratio of 1 µg DNA:2.5 µl Lipofectamine 2000 according to the manufacturer's instructions. Electrophysiology recordings were made 48 h post transfection.

Electrophysiology. Neurons whose cell bodies were not in contact with those of other neurons and transfected HEK293a cells tagged with fluorescent proteins were selected for recording. Currents were recorded using Axopatch 200B and Multiclamp 700 amplifiers (Axon Instruments, Molecular Devices Inc.). Pipettes were pulled from borosilicate glass capillaries with a P-97 puller (Sutter Instrument Co.)

with resistances of 2–4 MΩ. Currents were digitized with the Digidata 1322A and 1440A data acquisition systems (Axon Instruments, Molecular Devices Inc.). Data were captured using PClamp 8.1 & 10 software and analysed using ClampFit 10.2 (Axon Instruments). Currents were low-pass filtered at 5 kHz and sampled at 10 kHz. Capacity transients were cancelled, however, series resistance were not compensated. Voltages were not corrected for liquid junction potentials. Recordings were performed at room temperature. Recordings were carried out in the perforated patch configuration. The pipette solution contained (in mM) 110 CH_3COOK, 30 KCl, 5 NaCl, 1 $MgCl_2$ and 10 HEPES (pH corrected to 7.35 using KOH, osmolarity: ~310 mOsm with sucrose). 205 Mg per mililitre of fresh amphotericin B was added to this solution before recording. The bath solution contained (in mM): 140 NaCl, 4 KCl, 2 $CaCl_2$, 1 $MgCl_2$, 5 glucose and 10 HEPES (pH 7.4 adjusted using NaOH, osmolarity: ~320 mOsm with sucrose). 8-pCPT was added to the bath solution after establishment of a stable response to a 0.008 Hz mechanical stimulus. In HEK293 cells expressing Piezo1/2 either bath solution or 8-pCPT was added to the bath solution. Recordings were made 20–50 min after the addition of 8-pCPT at room temperature. For experiments in which cytosolic Ca^{2+} concentration was fixed, the conventional whole-cell configuration was used. Whole-cell patch clamp solution contained (in mM) KCl (130), $MgCl_2$ (2.5), $CaCl_2$ (1.94 or 4.63 to give 50 nM or 1 μM free Ca^{2+}), EGTA (5) K-ATP (3) HEPES (5) and pH 7.4 KOH (osmolarity was set to 310 mOsm with sucrose).

Mechanical stimulation. Mechanical stimulation of cell bodies was achieved using a heat-polished glass pipette (tip diameter ~2 μm), controlled by a piezo-electric crystal drive (Siskiyou MXPZT-300 series or Burleigh LSS-3000 series), positioned at an angle of about 70° to the surface of the dish. The probe was positioned so that a ~x μm (x = 10–14 μm) movement did not visibly contact the cell but that a x + 1 μm stimulus produced an observable membrane deflection. The probe was moved at a speed of 1 μm ms^{-1} and the stimulus was applied for 250 ms. A series of mechanical steps in ~1 (HEK cells) or ~2 μm (DRG neurons) increments were applied. Criteria for classifying adaptation kinetics of rapidly adapting mechanosensitive currents (RA) in DRG neurons had a decay kinetic that was best described by a bi-exponential fit[5]. Kinetics of adaptation to the mechanical stimuli were fitted with a standard mono exponential decay with the equation below using PClamp 10.2.

$$f(t) = \sum_{i=1}^{n} A_i e^{-t/\tau_i} + C$$

The fit solves for the amplitude A, the time constant τ, and the constant y-offset C for each component i.

Western blot analysis. DRG cultures were homogenized in ice-cold RAL lysis buffer (200 mM NaCl, 50 mM Tris–HCl (pH 7.5), 10% glycerol, 1% NP-40, 2 mM sodium orthovanadate, 2 mM phenylmethylsulfonyl fluoride and protease inhibitor mix (Sigma-Aldrich, p3840, 1:100)). Proteins were separated by SDS–polyacrylamide gel electrophoresis and transferred to PVDF membranes (Millipore, Bedford, MA, USA). Blots were stained with mouse-anti-Epac1 and as loading control rabbit-anti-β-actin or the neuron-specific mouse-anti-β3-tubulin (all cell signalling). Subsequently, blots were incubated with goat anti-mouse-peroxidase or donkey-anti-rabbit IgG + IgM (H + L) (GE Healthcare) and developed by enhanced chemiluminescence plus (Amersham Int.).

mRNA isolation and real-time PCR. Lumbar DRGs (L2-L5) were isolated and total RNA was isolated with RNeasy Mini Kit (Qiagen) in accordance with the manufacturer's instructions. Reverse transcription was performed with 1 μg of RNA by using iScript Select cDNA Synthesis Kit (Invitrogen). Real-time quantitative PCR was then performed with iQ SYBR Green Supermix (Invitrogen). The following primer pairs were used:

Epac1: 5′-gTgTTggTgAAggTCAATTCTg-3′ (forward), 5′-CCACACCACgggCATC-3′ (reverse)

Epac2: 5′-TgTTAAAgTgTCTgAgACCAgCA-3′ (forward), 5′-AAAggCTgTCCCAATTCCCAg-3′ (reverse)

Piezo1: 5′-CTACAAATTCgggCTggAg-3′ (forward), 5′-TCCAgCgCCATggATAgT-3′ (reverse)

Piezo2: 5′-CCAAgTAgCCCATgCAAAAT-3′ (forward), 5′-gCATAACCCTgTgCCAgATT-3′ (reverse)

β-Actin: 5′-AgAgggAAATCgTgCgTgAC-3′ (forward), 5′-CAATAgTgATgACCTggCCgT-3′ (reverse)

GAPDH: 5′-TgAAgCAggCATCTgAgg-3′ (forward), 5′-CgAAggTggAAgAgTgggAg-3′ (reverse)

Data analysis. Data are expressed as mean ± s.e.m. Measurements were compared using Student's t-test, one-way one-way analysis of variance (ANOVA), repeated measures, or two-way ANOVA followed by Bonferroni's analysis. A P-value of <0.05 was considered to be statistically significant.

References

1. Di Castro, A., Drew, L. J., Wood, J. N. & Cesare, P. Modulation of sensory neuron mechanotransduction by PKC- and nerve growth factor-dependent pathways. *Proc. Natl Acad. Sci. USA* **103,** 4699–4704 (2006).
2. Wood, J. N. & Eijkelkamp, N. Noxious mechanosensation-molecules and circuits. *Curr. Opin. Pharmacol.* **12,** 4–8 (2012).
3. Costigan, M., Scholz, J. & Woolf, C. J. Neuropathic pain: a maladaptive response of the nervous system to damage. *Annu. Rev Neurosci.* **32,** 1–32 (2009).
4. Coste, B. *et al.* Piezo1 and Piezo2 are essential components of distinct mechanically activated cation channels. *Science* **330,** 55–60 (2010).
5. Quick, K. *et al.* TRPC3 and TRPC6 are essential for normal mechanotransduction in subsets of sensory neurons and cochlear hair cells. *Open. Biol.* **2,** 120068 (2012).
6. Hucho, T. & Levine, J. D. Signaling pathways in sensitization: toward a nociceptor cell biology. *Neuron* **55,** 365–376 (2007).
7. Bos, J. L. Epac proteins: multi-purpose cAMP targets. *Trends Biochem. Sci.* **31,** 680–686 (2006).
8. Wei, F. *et al.* Genetic elimination of behavioral sensitization in mice lacking calmodulin-stimulated adenylyl cyclases. *Neuron* **36,** 713–726 (2002).
9. Pierre, S., Eschenhagen, T., Geisslinger, G. & Scholich, K. Capturing adenylyl cyclases as potential drug targets. *Nat. Rev. Drug Discov.* **8,** 321–335 (2009).
10. Yajima, Y. *et al.* Differential involvement of spinal protein kinase C and protein kinase A in neuropathic and inflammatory pain in mice. *Brain Res.* **992,** 288–293 (2003).
11. Malmberg, A. B. *et al.* Diminished inflammation and nociceptive pain with preservation of neuropathic pain in mice with a targeted mutation of the type I regulatory subunit of cAMP-dependent protein kinase. *J. Neurosci.* **17,** 7462–7470 (1997).
12. Grandoch, M., Roscioni, S. S. & Schmidt, M. The role of Epac proteins, novel cAMP mediators, in the regulation of immune, lung and neuronal function. *Br. J. Pharmacol.* **159,** 265–284 (2010).
13. Gloerich, M. & Bos, J. L. Epac: defining a new mechanism for cAMP action. *Annu. Rev. Pharmacol. Toxicol.* **50,** 355–375 (2010).
14. Holz, G. G., Kang, G., Harbeck, M., Roe, M. W. & Chepurny, O. G. Cell physiology of cAMP sensor Epac. *J. Physiol.* **577,** 5–15 (2006).
15. McCarter, G. C., Reichling, D. B. & Levine, J. D. Mechanical transduction by rat dorsal root ganglion neurons *in vitro*. *Neurosci. Lett.* **273,** 179–182 (1999).
16. Drew, L. J., Wood, J. N. & Cesare, P. Distinct mechanosensitive properties of capsaicin-sensitive and -insensitive sensory neurons. *J. Neurosci.* **22,** RC228 (2002).
17. Drew, L. J. *et al.* Acid-sensing ion channels ASIC2 and ASIC3 do not contribute to mechanically activated currents in mammalian sensory neurones. *J. Physiol.* **556,** 691–710 (2004).
18. Hu, J. & Lewin, G. R. Mechanosensitive currents in the neurites of cultured mouse sensory neurones. *J. Physiol.* **577,** 815–828 (2006).
19. Hao, J. & Delmas, P. Multiple desensitization mechanisms of mechanotransducer channels shape firing of mechanosensory neurons. *J. Neurosci.* **30,** 13384–13395 (2010).
20. Drew, L. J. & Wood, J. N. FM1-43 is a permeant blocker of mechanosensitive ion channels in sensory neurons and inhibits behavioural responses to mechanical stimuli. *Mol. Pain* **3,** 1 (2007).
21. Kimitsuki, T. & Ohmori, H. Dihydrostreptomycin modifies adaptation and blocks the mechano-electric transducer in chick cochlear hair cells. *Brain Res.* **624,** 143–150 (1993).
22. Cho, H., Shin, J., Shin, C. Y., Lee, S. Y. & Oh, U. Mechanosensitive ion channels in cultured sensory neurons of neonatal rats. *J. Neurosci.* **22,** 1238–1247 (2002).
23. Hucho, T. B., Dina, O. A. & Levine, J. D. Epac mediates a cAMP-to-PKC signaling in inflammatory pain: an isolectin B4(+) neuron-specific mechanism. *J. Neurosci.* **25,** 6119–6126 (2005).
24. Abrahamsen, B. *et al.* The cell and molecular basis of mechanical, cold, and inflammatory pain. *Science* **321,** 702–705 (2008).
25. Ferrari, L. F., Chum, A., Bogen, O., Reichling, D. B. & Levine, J. D. Role of Drp1, a key mitochondrial fission protein, in neuropathic pain. *J. Neurosci.* **31,** 11404–11410 (2011).
26. Eijkelkamp, N. *et al.* Low nociceptor GRK2 prolongs prostaglandin E2 hyperalgesia via biased cAMP signaling to Epac/Rap1, protein kinase C{varepsilon}, and MEK/ERK. *J. Neurosci.* **30,** 12806–12815 (2010).
27. Djouhri, L. & Lawson, S. N. Abeta-fiber nociceptive primary afferent neurons: a review of incidence and properties in relation to other afferent A-fiber neurons in mammals. *Brain Res. Brain Res. Rev.* **46,** 131–145 (2004).
28. Zhu, Y. F. & Henry, J. L. Excitability of abeta sensory neurons is altered in an animal model of peripheral neuropathy. *BMC Neurosci.* **13,** 15 (2012).
29. Oestreich, E. A. *et al.* Epac and phospholipase cepsilon regulate Ca2+ release in the heart by activation of protein kinase cepsilon and calcium-calmodulin kinase II. *J. Biol. Chem.* **284,** 1514–1522 (2009).